

Advances in GaN-on-Glass for Optoelectronic Devices: Progress in Epitaxial Growth, Device Integration, and Applications

Jungwook Min and Kwangwook Park*

GaN-on-glass epitaxy technology has transformed the landscape of optoelectronic device fabrication, providing scalable and cost-effective solutions for next-generation optoelectronic applications. Amorphous glass, characterized by large-area scalability, transparency, and low cost, presents various challenges, such as the absence of global epitaxy. Advances in epitaxial methods have facilitated the growth of high-quality GaN thin films and nanostructures on glass substrates. The integration of preorienting layers improves crystallinity, in-plane symmetry, and device functionality. These advancements have led to the successful fabrication of GaN-based light-emitting diodes, photodetectors, and hybrid heterostructures for full-color displays, integrated systems, and energy-efficient devices. Innovations in material compatibility and heterostructure designs allow precise control over crystal orientation and defect densities, thereby pushing the boundaries of optoelectronic performance. This review highlights the current progress in GaN-on-glass technology and emphasizes its transformative role in optoelectronics. By reflecting on these advancements and their applications, this review underscores the potential of GaN-on-glass as a cornerstone for high-performance, sustainable optoelectronic devices.

optoelectronic applications. These semiconductors offer significant advantages, such as high chemical stability,^[3] excellent electron mobility,^[4] and large piezoelectric coefficients.^[5] Traditionally, group-III nitrides are grown on single-crystal substrates such as sapphire, silicon, and silicon carbide (SiC). However, these substrates are expensive and have a limited wafer size.^[6] For future applications in next-generation displays, solar cells, and lighting, large-scale and low-cost substrates are critical, with amorphous glass emerging as the most promising candidate.

Glass substrates offer notable advantages such as freedom from size limitations, low cost, and high optical transparency.^[7] However, the amorphous nature of glass poses significant challenges to the growth of single-crystal group-III nitride semiconductors because they lack a crystalline structure to support global epitaxy. In addition, the low thermal conductivity of glass introduces operational challenges in device inte-

gration. To overcome these limitations, researchers have explored the properties of polycrystalline GaN grown on glass substrates using various epitaxial methods. To achieve high crystallinity, specifically global epitaxy and in-plane rotational symmetry of GaN, preorienting layers composed of group-III nitride buffers, metals, and 2D materials have been developed and integrated into the growth process.


These efforts have resulted in significant progress, culminating in the successful implementation of optoelectronic devices such as light-emitting diodes (LEDs) and photodetectors (PDs) on glass substrates. This review introduces the epitaxial growth and characterization techniques employed for GaN growth on amorphous substrates in Section 2. Section 3 discusses the growth of GaN crystals on bare glass, while Section 4 focuses on GaN crystal growth on glass coated with preorienting layers, along with its applications in optoelectronic devices.

1. Introduction

Group-III semiconductors are essential for the fabrication of optoelectronic devices. As direct-bandgap materials, they span a wide spectral range, from infrared (0.68 eV) to UV (6.2 eV), for optoelectronic applications,^[1,2] making them ideal for various

J. Min
Department of Optical Engineering
Kumoh National Institute of Technology
Gumi 39253, Republic of Korea

K. Park
Division of Advanced Materials Engineering
Division of Electronics and Information Engineering
Hydrogen and Fuel Cell Research Center
Jeonbuk National University
Jeonju 54896, Republic of Korea
E-mail: kwangwook.park@jbnu.ac.kr

 The ORCID identification number(s) for the author(s) of this article can be found under <https://doi.org/10.1002/adpr.202500014>.

© 2025 The Author(s). Advanced Photonics Research published by Wiley-VCH GmbH. This is an open access article under the terms of the Creative Commons Attribution License, which permits use, distribution and reproduction in any medium, provided the original work is properly cited.

DOI: 10.1002/adpr.202500014

2. Growth and Characterization of GaN-on-Glass

2.1. Characteristics of Amorphous Glass Substrate

Recent studies have explored the direct growth of GaN on amorphous glass substrates. Unlike crystalline substrates, glass is not restricted by size and serves as an electrical insulator, making it

suitable for large-area displays and optoelectronic devices. Applications include GaN-based micro-LED arrays on large panels and glass substrates as interposers for semiconductor packaging.^[8] However, lattice matching during GaN growth is inherently difficult because of the absence of a lattice structure in the glass, leading to a relatively low crystal quality of GaN. In addition, certain types of glass exhibit limited thermal stability during high-temperature processing. Hence, understanding the manufacturing methods and intrinsic properties of glass substrates is essential for advancing the GaN-on-glass technology. This section begins with an overview of the various compositions and evaluations of technical glass substrates (Section 2.1.1), followed by a focused examination of the properties of typical SiO₂-based glass (fused silica) in Section 2.1.2. Section 2.1.3 discusses how the electrical and thermal properties of glass substrates influence the operational stability, signal response, thermal behavior, and lifetime of GaN-based devices, highlighting the critical need for effective thermal management and device design strategies. In this discussion, we aim to identify the advantages and drawbacks of amorphous glass substrates as GaN growth platforms.

2.1.1. Technical Glass Substrates: Key Characteristics and Evaluation

“Technical glass” refers to high-purity and low-defect glass materials specifically tailored for targeted properties, such as minimal thermal expansion, excellent transparency, or enhanced mechanical strength.^[9] These modifications enable them to play diverse roles in optical windows, display panels, semiconductor fabrication equipment, and photomask substrates. Major manufacturers such as Corning Inc., SCHOTT AG, and AGC Inc. (Asahi Glass) supply a range of technical glass products, most commonly based on silica (SiO₂), borosilicate, or aluminosilicate compositions, each suited to specific thermal and chemical resistance requirements.^[8] Although SiO₂-based glass is the most widely used, other variants such as phosphate or chalcogenide glass can be adapted to specific fields, including IR optics and biomedical applications.^[10] Glass ceramics undergo controlled crystallization to significantly improve their mechanical and thermal properties. Notable examples include compositions containing β -quartz or gahnite (ZnAl₂O₄), which can remain transparent if either the crystallite size is considerably smaller than visible wavelengths or if the refractive index mismatch between the crystal and glass is minimized.^[11]

Technical glass is typically evaluated in terms of its coefficient of thermal expansion (CTE), softening point, chemical durability, and optical transmission spectrum. These properties must meet the stringent demands of semiconductor fabrication, including repeated thermal cycles, corrosive etchants, and dimensional precision.^[8] Large-format planarization and polishing further expand its utility in big-screen display substrates, photomasks, and glass interposers. Certain glass-ceramic products exhibit low thermal expansion and high toughness, making them potential substrates for advanced semiconductor packaging. In GaN-on-glass research, low-alkali or high-temperature-resistant glass materials (e.g., Corning EAGLE XG) are introduced to survive processing temperature beyond 600–700 °C. By suppressing issues such as sodium ion diffusion, researchers can deposit

GaN thin films across large areas at a relatively lower cost. These developments have drawn attention to next-generation displays and optoelectronics, where glass-based GaN can enable a broad range of new applications.^[8]

To assess the suitability of glass materials as substrates for the GaN-on-glass approach, it is essential to review both commercially available high-performance glass products and the industry standards that define their properties. Table 1 summarizes key examples of alkali-free glass substrates commonly used in semiconductor and display applications. It includes a brief description of their characteristics and uses, source links (to official product documentation or standard references), remarks on their compatibility with GaN growth, and relevant American Society for Testing and Materials (ASTM) standards. Standard test methods and specifications have been established to consistently evaluate the physical, chemical, and mechanical properties of various materials and are widely adopted by both research institutions and industry. By adhering to these ASTM standards, material performance can be assessed uniformly across different laboratories, thereby improving the reliability and reproducibility of results in GaN-on-glass research. ASTM standards are especially relevant for evaluating glass material properties as well. For example, the CTE of glass substrates is quantitatively measured using a push-rod dilatometer in accordance with ASTM E228. The softening point is determined using ASTM C338, commonly known as the Littleton softening point test. Additionally, ASTM C336 is employed to assess the annealing point and glass transition temperature. Other relevant standards address mechanical strength (e.g., flexural strength via ASTM C158), chemical durability (e.g., acid and alkali resistance tests), and optical transmittance. In short, the thermal, mechanical, and chemical stability of technical glass can be rigorously evaluated using ASTM standard tests. These categories align closely with the key properties discussed earlier—thermal expansion, softening behavior, chemical resistance, and optical transmission—and serve as critical indicators for identifying glass materials suitable for GaN-on-glass applications.

In the context of GaN-on-glass research, consideration of ASTM standards is crucial. To enable uniform deposition of GaN thin films over large areas, the glass substrate must retain its structural integrity and dimensional stability under high-temperature processing and withstand repeated thermal cycling and etching. Because GaN growth typically involves elevated temperatures, evaluating the softening point and deformation (strain) behavior of glass according to ASTM protocols is necessary. Furthermore, to prevent contamination from alkali ions diffusion—particularly sodium—low-alkali glass is preferred. Its chemical composition and durability should also be validated using ASTM-standard test. Ultimately, ASTM standards provide a scientific basis for selecting appropriate glass materials for GaN-on-glass integration and for optimizing related process conditions. They play a critical role in ensuring the long-term reliability required for next-generation displays and optoelectronic devices. Based on this context, the following table summarizes representative commercial technical glass products and their corresponding ASTM standards.

As shown in Table 1, modern display-grade glasses (e.g., Corning EAGLE XG, SCHOTT AF 32 eco, and AGC EN-A1) share several advantageous properties. They are free of alkali impurities—minimizing contamination during semiconductor

Table 1. Overview of representative alkali-free glass substrates, relevant ASTM standards, and manufacturer resources, including notes on suitability for GaN film growth.

Item	Description (key characteristics and applications)	Remarks (GaN growth suitability and CVD/PVD applicability)
Corning EAGLE XG ^[112] <i>Alkali-free display glass</i>	A high-quality, alkali-free boroaluminosilicate glass substrate developed for flat panel displays and electronic applications. It provides excellent dimensional stability, low density, and a CTE closely matched to that of silicon. Free of added heavy metals, it has a stain point of ≈ 665 – 670 °C, allowing for moderately high-temperature processing without warping or devitrification during standard display fabrication. Widely used in TFT-LCD, OLED, and emerging micro-LED applications.	Tolerates moderate thermal processes (≈ 600 – 700 °C); however, standard high-temperature GaN MOCVD (> 900 °C) may exceed its softening point (≈ 900 – 950 °C), risking deformation. Consequently, direct epitaxy is challenging. Nonetheless, it can still support GaN film deposition using lower-temperature method such as sputtering, typically yielding polycrystalline films.
SCHOTT AF 32 eco ^[113] <i>Ultra-thin semiconductor glass</i>	An alkali-free thin glass produced using down-draw technology, characterized by high surface quality and a thermal expansion coefficient ($\approx 3.2 \times 10^{-6}$ K ⁻¹) closely matched to that of silicon. It has a high glass transition temperature (717 °C) and is suitable for processes up to ≈ 600 °C, supporting wafer-level packaging and MEMS integration. Its low alkali content, excellent surface smoothness, and dimensional stability make it ideal for sensor windows, interposers, and optical applications.	Suitable for deposition processes below ≈ 600 °C (e.g., sputtering, plasma-enhanced CVD [PECVD]), but not for conventional MOCVD at ≈ 1000 °C. As with other amorphous substrates, the resulting films will be polycrystalline unless specialized buffer layers or intermediate processes are employed.
AGC EN-A1 ^[114] <i>Alkali-free interposer glass</i>	A high-transmittance boroaluminosilicate glass designed for advanced packaging, microfluidics, and display applications, featuring a thermal expansion coefficient of $\approx 3.8 \times 10^{-6}$ K ⁻¹ , closely matched to that of silicon. Optimized for through-glass vias (TGV) with minimal tapering, it provides excellent chemical durability and thermal stability, with a glass transition temperature of 700 °C and a softening point of 950 °C. Commonly used in wafer-level optics, sensor wafers, and micro-LED packaging as a transparent and dimensionally stable platform.	Although mechanically robust, its glass transition temperature (≈ 700 °C) limits sustained exposure temperature above 900 °C. Conventional GaN epitaxy is typically too high in temperature, posing a risk of warping. Nonetheless, EN-A1 can support low-temperature GaN deposition via sputtering or plasma-assisted CVD.
ASTM E228-22 ^[115] <i>Standard Test Method for Linear Thermal Expansion of Solid Materials</i>	Measures the linear CTE using a push-rod dilatometer from -180 to 900 °C.	Used to evaluate CTE mismatch between GaN and the glass; such mismatch can induce stress and lead to cracking during cooling.
ASTM C338-24 ^[116] <i>Standard Test Method for Softening Point of Glass</i>	Defines the softening point as the temperature at which a glass fiber elongates at a rate of 0.1 mm/min under its own weight; this is used to determine the maximum safe processing temperature.	It is important to ensure that GaN growth temperature (typically ≈ 1000 °C) remains below the glass softening point, as deformation during growth can degrade film quality.
ASTM C225-85 ^[117] <i>Standard Test Methods for Resistance of Glass Containers to Chemical Attack</i>	Assesses glass resistance to acidic and neutral environments through leaching and titration methods.	GaN-on-glass substrates undergo chemical etching and cleaning; chemical stability is essential to ensure durability and prevent surface degradation.
ASTM C1036-25 ^[118] <i>Standard Specification for Flat Glass</i>	Specifies visual quality grades for flat glass, including allowable limit for surface defects, bubbles, and edge chips.	Surface cleanliness and flatness are critical for defect-free GaN, as even minor flaws may initiate dislocations in GaN film.
ASTM C657-24 ^[119] <i>Standard Test Method for Volume Resistivity of Glass</i>	Determines the electrical resistivity of glass to assess its insulating performance under DC voltage.	High insulation is essential for GaN-on-glass applications in RF and power devices to minimize leakage current.
Corning ^[120]	Corning specializes in high-performance glass solutions for displays, optics, and semiconductor applications. Their fusion-draw process produces uniform, ultra-smooth substrates (e.g., EAGLE XG, Lotus series) widely used in LCD and OLED panels. Corning also manufactures HPFS fused silica, a high-purity material used in advanced optical system and photomask applications.	Corning's product portfolio ranges from standard display glass to specialized ultra-low-expansion glass for lithography. Each product has specific thermal limits, which may or may not align with GaN-on-glass growth requirements. To enable direct GaN epitaxy on glass, additional strategies such as low-temperature growth, engineered buffer layers, or wafer bonding techniques may be necessary.
AGC Inc. ^[121]	AGC produces a wide range of display and functional glasses, including the AN series for large-format panels and the EN series for electronic packaging, as well as architectural glass. Their focus on alkali-free boroaluminosilicate compositions supports applications requiring minimal ionic contamination, such as semiconductor processing. TGV-formable glass variants are suitable for advanced packaging and microelectronic integration.	As a core supplier to major display manufacturers, some AGC glasses are already used in micro-LED backplanes. However, direct GaN epitaxy is generally constrained by the thermal budget of the glass. For large-area GaN-on-glass applications, low-temperature deposition methods or bonding-based integration may be necessary.

Table 1. Continued.

Item	Description (key characteristics and applications)	Remarks (GaN growth suitability and CVD/PVD applicability)
SCHOTT AG ^[122]	SCHOTT is recognized for its specialty glass and glass-ceramics, including AF 32 eco, BOROFLOAT, and Zerodur. Its thin glass products are tailored for use in semiconductor packaging, imaging sensors, and microfluidics. SCHOTT also produces various grades of fused silica and ultra-low CTE glass-ceramics for precision optics and wafer-level integration.	SCHOTT's ultra-thin glasses enable large-scale MEMS and wafer-level packaging. In addition to MEMS-compatible thin glass, synthetic fused silica is offered for high-temperature lithography and high-power laser optics. While the thermal and compositional constraints of these materials may limit their use in direct GaN growth, they remain viable candidate for GaN-on-glass integration through low-temperature coating or transfer-based approaches.

processing—and exhibit thermal expansion coefficients closely matched to that of silicon. Additionally, they offer high optical quality and stringent dimensional tolerances, making them well-suited for large-area thin-film integration. However, a fundamental limitation is their relatively low tolerance to high temperatures; strain points typically range from ≈ 600 to 700°C , and softening points from ≈ 900 to 950°C . Conventional GaN metal–organic chemical vapor deposition (MOCVD) growth is performed near 1000°C , posing a risk of substrate deformation. Consequently, amorphous glass substrates often require reduced-temperature deposition methods, such as sputtering, which produce polycrystalline GaN over large areas. While such approaches do not yield single-crystalline film, they offer scalable and cost-effective pathways for emerging display and sensor technologies. The ASTM standards (E228, C338, C225, C1036, and C657) provide fundamental guidelines for assessing glass properties—including thermal expansion, softening point, chemical durability, surface quality, and electrical insulation. While useful for general glass selection, these standards only partially address the stringent requirements of GaN-on-glass growth, which demands high-temperature resilience, surface flatness, and compatibility with epitaxial processes.

2.1.2. SiO_2 Glass (Fused Silica): Properties and Semiconductor Applications

Fused silica is widely recognized as one of the purest and most durable glass materials. Owing to its exceptionally strong Si–O bonds, it demonstrates outstanding thermal and chemical stability, thus earning its reputation as a premier substrate for optical and semiconductor applications.^[8] Optically, high-purity fused silica maintains excellent transmittance ranging from deep UV ($\approx 180\text{ nm}$) to mid-infrared ($\approx 2.7\text{ }\mu\text{m}$), while its relatively low refractive index (≈ 1.46) and high laser damage threshold allow for diverse high-precision photonic uses.^[12] In terms of thermal behavior, its linear expansion coefficient ($\approx 0.5 \times 10^{-6}\text{ K}^{-1}$) is significantly lower than that of borosilicate or soda-lime glass, resulting in minimal distortion even under rapid heating or cooling.^[13] Its softening point ($\approx 1660^\circ\text{C}$) far exceeds that of most metals or ceramics, thereby preserving structural integrity throughout the demanding steps in semiconductor manufacturing. Along with an approximate bandgap of 9 eV , fused silica serves as a robust electrical insulator capable of sustaining high resistivity at elevated temperatures. Furthermore, its chemical inertness, which allows it to resist nearly all acids and bases except HF, broadens its range of industrial applications.

The large-area scalability of fused silica is a major advantage in the semiconductor field. Manufacturers can produce cylindrical ingots and slice them into 300 mm wafers or larger panels, and then employ laser or ultrasonic drilling and chemical etching to form fine vias and patterns. Such machinability enables developments such as glass interposers, where the moderate thermal conductivity and superior electrical insulation of fused silica improve both high-frequency performance and heat dissipation.^[8] For the applications in GaN-on-glass research, it typically withstands short high-temperature steps (up to $\approx 1000\text{--}1100^\circ\text{C}$) without substantial deformation. With well-established supply chains and refined processing methods, fused silica is likely to remain the key to next-generation GaN-on-glass technologies.

2.1.3. Effect of Glass Properties on GaN Device Performance

In addition to the limitations of GaN growth because of the absence of a lattice structure, certain types of glass have limited thermal stability under high-temperature processes, further complicating GaN-on-glass implementation. Consequently, understanding the electrical and thermal properties of glass substrates is essential for advancing the device-level performance in GaN-on-glass technology. Because the glass has high insulation and negligible electrical conductivity, GaN-based devices on glass, for example, those related to optoelectronic or power applications, have the advantage of minimizing the substrate leakage paths. In the case of large-scale micro-LED displays composed of pixels, such insulating properties help reduce pixel-to-pixel crosstalk and enable truly independent operation. In addition, because glass has a relatively low dielectric constant (≈ 3.8 for fused silica), parasitic capacitances can be lower, which mitigates RC delays or signal distortion in high-frequency circuits.

One of the fundamental drawbacks of glass substrates is their very low thermal conductivities. Typical silica-based glass exhibits a thermal conductivity of $\approx 1\text{--}1.3\text{ W m}^{-1}\text{ K}^{-1}$, significantly below sapphire ($25\text{--}35\text{ W m}^{-1}\text{ K}^{-1}$), SiC ($>300\text{ W m}^{-1}\text{ K}^{-1}$), or even Si ($\approx 130\text{ W m}^{-1}\text{ K}^{-1}$). Consequently, the heat generated during device operation cannot easily dissipate through the substrate, causing the local temperature to increase within the junction. A prior study assessed the time to 50% output decay of an InGaN LED at 85°C , revealing that a device on a patterned sapphire substrate lasted $\approx 590\text{ h}$, whereas one on standard sapphire survived for only 305 h .^[14] Considering that glass has an even lower thermal conductivity, its LED lifetime may decrease further without suitable heat management. In micro-LED arrays, substrate-driven heat conduction is crucial for micro-LED arrays.

An experiment showed that transferring the same micro-LED design from a diamond heat spreader (which operated stably for up to $\approx 10 \text{ W cm}^{-2}$) onto a glass substrate caused thermal roll-over at $\approx 3.2 \text{ W cm}^{-2}$, reducing the optical power density to nearly one-third of that achieved with the diamond heat spreader.^[15] Thermal imaging confirmed the presence of pronounced hotspots around the device. Such thermal build-up severely degrades the reliability and performance, requiring effective heat-spreading solutions (e.g., heat sinks or thin substrate strategies).

Instead of direct growth on glass, GaN LEDs grown on sapphire can be released via laser lift-off and bonded onto glass, allowing the device to retain the advantages of high-quality GaN while exploiting the transparency of glass or large panel form factors.^[16] This approach supports backside emission or flip-chip layouts that improve heat conduction; however, additional high-thermal-conductivity adhesives or backside coatings are essential. GaN high-electron-mobility transistors (HEMTs) can also be transferred onto glass; however, device self-heating becomes a limiting factor in high-power switching, restricting their practical usage to low-power or pulsed operations unless sophisticated cooling structures are adopted.^[17] Over 1 W of heat in a few mm^2 of the channel area may elevate the channel temperature by tens of degrees, impairing both the performance and device lifetime.^[18–20]

A low thermal conductivity often leads to local heating and reliability concerns. However, glass substrates offer excellent insulation, optical transparency, and cost-effective large-area scalability, enabling novel applications in GaN-based devices, such as micro-LED displays and backside-illuminated sensors. Notably, recent demonstrations of GaN LEDs on glass reaching 80%–90% of sapphire-based device efficiency, as well as high-resolution transparent micro displays via GaN-based micro-LED transfer, highlight the feasibility of glass substrates for practical GaN devices, provided that thermal and electric field management are sufficiently addressed.^[21,22]

2.2. GaN-on-Glass Growth Methods

Epitaxial GaN can be grown using various chemical vapor deposition (CVD) techniques, such as MOCVD,^[23] hydride vapor phase epitaxy (HVPE),^[24] and atomic layer deposition (ALD),^[25] as well as physical vapor deposition (PVD) techniques, including sputtering deposition,^[26] molecular beam epitaxy (MBE),^[27] and pulsed laser deposition (PLD).^[28] However, not all deposition techniques are suitable for GaN growth because an active nitrogen-rich environment is required for the reaction with gallium. This environment is typically achieved by using NH_3 or plasma-activated nitrogen to facilitate GaN growth. In this section, epitaxial GaN growth methods are introduced, followed by a discussion of GaN crystal quality.^[29]

2.2.1. Growth Using CVD Methods

MOCVD is the most widely used technique for growing GaN crystals in the compound semiconductor industry. It involves reacting metal-organic precursors (e.g., trimethylgallium, TMGa) and ammonia (NH_3) at high temperatures to form

GaN thin films and is also employed in commercial LED production. Typically, growth temperatures near 1000°C are required to achieve high-quality epitaxial layers on single-crystal substrates such as sapphire or SiC. However, glass substrates generally have poor thermal properties, making it difficult to directly apply such high-temperature processes. For instance, large-area, alkali-free display glass often exhibits a softening point of 970°C and strain point of $\approx 670^\circ\text{C}$; therefore, temperatures above 600°C can lead to substrate deformation or thermal damage. In addition, typical glass contains a considerable number of alkali ions (e.g., Na), which can diffuse to the surface during high-temperature processes and be incorporated into the growing GaN layer. Consequently, to realize GaN-on-glass, low-temperature growth is essential, and direct growth at high temperatures often results in randomly oriented polycrystalline GaN films. Various approaches have been explored to address these issues. One strategy involves depositing a thin Ti metal film on a glass surface to induce crystal orientation, forming a GaN nucleation layer at low temperatures, followed by conventional high-temperature GaN growth via MOCVD.^[30] This method enables localized single-crystal-like growth of GaN on amorphous glass and can ultimately produce LEDs with a performance comparable to that of GaN grown on sapphire substrates.

In addition to MOCVD, HVPE is another major CVD technique for GaN growth. In HVPE, GaCl vapor species generated by the reaction of metallic Ga with HCl subsequently react with NH_3 to grow GaN. HVPE has been used to grow thick GaN layers and fabricate GaN substrates. It can achieve a rapid growth rate, often exceeding a few hundred micrometers per hour, which makes it suitable for producing freestanding or bulk GaN substrates. For example, Kim et al. reported the growth of a thick GaN layer on fused silica via HVPE, followed by the removal of the glass substrate by chemical etching to obtain a $20 \times 20 \text{ m}^2$ freestanding GaN substrate.^[31] Despite these advantages in thick-layer fabrication, HVPE also requires very high temperatures ($>1000^\circ\text{C}$), posing severe challenges for common glass substrates such as borosilicate or soda-lime glass, which tend to soften or crack, while alkali ion diffusion further deteriorates crystal quality. Yu et al. noted that the diffusion and reaction of substrate elements affect GaN crystal formation during HVPE on Si substrates, and these issues are even more severe with glass.^[32] Consequently, the application of HVPE to GaN-on-glass is quite limited; with specialized high heat resistance, alkali-free glass (such as fused silica) can sometimes be used, or the glass can be removed to obtain freestanding GaN.

Various strategies have been investigated to mitigate the problems arising from these high-temperature processes on glass substrates, including buffer layers that alleviate the thermal expansion mismatch and block impurity diffusion from the substrate. For example, a thin low-temperature AlN or GaN nucleation layer is routinely used when growing GaN on sapphire, a concept that can also be extended to glass by depositing a thin SiN_x or AlN buffer layer, or by performing NH_3 plasma pretreatment to nitride the glass surface.^[33] Sato et al. fabricated an InGaN/GaN thin film on glass by slowly growing a GaN layer below 500°C to form a polycrystalline film, which slightly increased the temperature to improve crystal growth. Although lowering the process temperature generally leads to a somewhat reduced crystal quality, it prevents substrate damage, making it feasible to use glass.^[34] Another approach is to use alkali-free substrates with

improved chemical composition to minimize Na diffusion; recent display technologies have introduced Eagle XG and Willow Glass, which are largely free of Na and K and can be used up to ≈ 600 – 700 °C. Such substrates can reduce defect formation in the growing GaN layer, thereby facilitating the fabrication of glass-based LEDs.

To successfully implement GaN-on-glass via CVD, inducing substrate-friendly conditions such as low-temperature nucleation, surface nucleation, and buffer-layer insertion to block diffusion is crucial. Even with these conditions, the resulting GaN film is usually polycrystalline; nevertheless, it can exhibit a preferential *c*-axis orientation. Further process optimization of multistep approaches may gradually enhance crystal quality.

2.2.2. Growth Using PVD

In addition to chemical reactions, growth techniques based on physical evaporation or sputtering have been explored for GaN-on-glass. Examples include MBE, PLD, and pulsed sputtering deposition (PSD). These PVD methods typically require relatively low growth temperatures and feature simple configurations. In MBE, for example, Ga metal evaporates under ultra-high vacuum and reacts with activated nitrogen (e.g., a plasma source) to achieve epitaxial growth, allowing GaN thin film growth at ≈ 600 – 800 °C. PLD and PSD (such as magnetron sputtering) can form films at even lower temperatures, often below 300 – 500 °C, making them attractive for thermally sensitive glass substrates. However, low-temperature growth typically leads to inferior crystallinity. On noncrystalline substrates such as glass, the grains often nucleate randomly, producing polycrystalline or quasi-amorphous films. Zou et al. reported that GaN grown on glass via mid-frequency sputtering exhibited an X-ray diffraction (XRD) (002) rocking curve with a full width at half maximum (FWHM) of several degrees, indicating poor crystal ordering.^[35] Furthermore, PVD-grown GaN often exhibits columnar growth, in which grains nucleate randomly at the surface and grow vertically in pillar-like structures, leading to a lack of uniform in-plane orientation.

Various methods have been proposed to overcome these limitations. First, plasma-assisted molecular beam epitaxy (PA-MBE) employs nitrogen plasma to enhance the generation of active species and increase the surface mobility, enabling crystal growth at lower temperatures.^[36] For example, some studies have explored growing GaN nanocolumns at ≈ 500 °C by PA-MBE, and then attempting to coalesce these nanocolumns into a more oriented film.^[37] Second, the incorporation of a thin buffer layer during the initial nucleation stage is beneficial. Liu et al. introduced a thin ZnO buffer film during pulsed DC sputtering to improve GaN grain size and orientation on glass, resulting in stronger (002) texture at a low growth temperature of ≈ 300 °C.^[38] Because ZnO has a wurtzite structure similar to that of GaN and good adhesion to glass, it forms an effective interfacial layer. Additional methods include plasma pretreatment of the glass surface to enhance the chemical reactivity or introduce nitrogen, as well as providing supplemental energy (e.g., ion beams) during deposition to promote surface migration at low temperatures. Ion-beam-assisted deposition (IBAD) is a well-known example of reducing the defect density in TiN films via low-energy ion assistance.^[39] When applied to GaN, similar ion energy inputs can

favor oriented crystal nucleation. An increased plasma density drives more frequent particle collisions and thus improves film crystallinity, even at low temperatures. This technique blends elements of both chemical and physical deposition to achieve crystalline thin films at temperatures well below those used in conventional CVD.

The PVD method is actively exploring additional techniques, such as buffer layer insertion, plasma or ion-beam assistance, and other enhancements, to preserve the low-temperature advantages while improving GaN crystallinity on glass. **Table 2** lists the different growth methods for achieving GaN-on-glass, each with intrinsic tradeoffs that lead to considerable variation in the crystal quality. High-temperature CVD can attain superior crystallinity but has low compatibility with common glass substrates, whereas low-temperature PVD is more substrate-friendly but typically yields poorer crystal quality.

2.3. GaN-on-Glass Growth Technology

For large-area glass-based optoelectronics, developing a hybrid approach that prevents substrate damage while maximizing the crystal quality of GaN is crucial. This section focuses on improving the orientation and crystallinity of GaN-on-glass using methods such as preorienting layers, local and global epitaxy concepts, and the insertion of metal-based orientation films with fine patterning for selective area growth (SAG). By employing these strategies, nearly single-crystalline GaN thin films can be realized even on amorphous glass, and their feasibility for devices can be assessed.

2.3.1. GaN-on-Glass Preparation Methods and Characterization of GaN

As with crystalline substrates, the surface cleanliness and initial orientation are crucial for GaN growth on glass. First, the glass substrate is cleaned using organic solvents to remove particles and residual organics. Sequential cleaning with acetone, methanol, and isopropanol reduces the surface contamination. Additional plasma cleaning or UV–ozone treatment can be applied to eliminate the remaining hydrocarbons completely. After cleaning, a pretreatment step involving a group-V source can be performed in the reactor of an MOCVD or MBE system to modify the substrate surface. For example, annealing the substrate under an NH_3 atmosphere, the so-called nitridation, can form a nitride layer on the glass surface, creating favorable conditions for initial GaN nucleation. For the sapphire substrate, the nitridation forms a thin AlN layer that enhances the lattice matching of GaN.^[33] Similarly, for amorphous glass substrates, some Si–O bonds are replaced by Si–N, which provide nucleation sites.^[40] By combining solvent cleaning and nitridation pretreatment, the glass surface exhibited improved cleanliness and chemical activity, which stabilized the GaN nucleation in the early growth stage. In contrast, if no pretreatment is conducted, then residual contaminants or moisture on the glass surface can interfere with crystallization, leading to smaller grains and randomly oriented polycrystalline phase.^[34] Therefore, optimizing pretreatment conditions, such as surface cleaning and nitridation, is essential for achieving high-quality GaN-on-glass.

Table 2. Comparison of key GaN thin film growth techniques for GaN-on-glass.

Growth method	Growth temp.	Growth rate ($\mu\text{m}/\text{h}$)	Applicable substrates/temp. limit on glass	Crystal quality, X-ray rocking curve on sapphire, and crystal quality on glass	Advantages and disadvantages
MOCVD	900–1100 °C (low-temp. nucleation at ≈ 500 °C)	≈ 1 –5	Single-crystal substrates (sapphire, SiC, Si, etc.) / General glass only up to ≈ 600 °C (due to softening and Na diffusion at higher temp.)	on sapphire: Epitaxial quality (single crystal), hundreds of arcsec (002) on glass: polycrystalline (<i>c</i> -axis preferred orientation, in-plane disorder)	Uniform large-area growth, proven industrial use at atmospheric pressure, ability to control complex compositions Requires ≈ 1000 °C high-temperature process, high precursor costs, thermal damage risk for glass substrates
HVPE	1000–1100 °C	10–200	Requires high-temp.-resistant substrates (GaN templates or sapphire) / Some research has used fused silica glass, ^[31] incompatible with general glass (softening & chemical reactions)	on sapphire: Thick-film high quality, (002) a few tens to a few hundred arcsec for films a few micrometers thick on glass: <i>c</i> -axis-oriented polycrystal (grain boundaries present)	Very rapid growth rate, capable of thick layers that reduce defects (practical route to bulk GaN) Handling issues due to HCl corrosion, difficult to control alloy composition, rough surface, challenging direct growth on glass (high temperatures)
PA-MBE	600–800 °C	0.1–1	Epitaxy on single-crystal substrates (Si, sapphire, etc.)/Possible at lower temp., but no lattice matching on glass cause nanocolumns or amorphous films	on sapphire: High quality when lattice-matched, hundreds of arcsec, defect density $\approx 10^8$ – 10^9 cm ² (002) on glass: crystallites do not form well (nanocolumn or polycrystalline)	Precise thickness/composition control at the atomic layer level, easy doping profiling, relatively low growth temperature possible Very slow growth rate, expensive equipment, limited uniformity over large areas, industrial mass production is challenging
PLD	RT–700 °C	≈ 0.1 –1 (depends on laser repetition rate)	Compatible with a wide variety of substrates (flat, curved, etc.)/Glass substrates are easily used (≤ 500 °C)	on sapphire: polycrystalline or quasi-single-crystal, crystal grain size of a few tens of nm, preferred orientation possible on glass: in-plane orientation is random; local texture can form	Easy to deposit various materials in a lab setting (not only GaN but also oxides, etc.), free control of composition by changing targets, relatively low temperature Particle defects from laser ablation, limited deposition area due to the plume, reproducibility issues
Pulsed/RF magnetron sputtering (PSD)	RT–500 °C	≈ 0.1 –0.5 (depends on target power)	Can be deposited on most substrates (glass, plastic, etc.)/Large-area process possible and thin films can be formed below 400 °C (compatible with flat-panel display methods)	on sapphire: tends toward polycrystalline or amorphous, several degrees (002) on glass: vertically oriented columnar grains (≈ 20 –50 nm) ^[38]	Relatively low equipment cost, simple and stable process, low-temperature deposition minimizes substrate damage, suitable for large-scale production Incomplete nitridation under certain conditions can lead to N-vacancies and oxygen impurities (due to pressure environment), small crystal grains degrade electrical properties, difficult to grow thick films (stress)
Plasma-enhanced atomic layer deposition (PEALD)	100–300 °C	a few nm/h	Can be used on virtually any substrate/Excellent uniformity over large areas (precise atomic-layer thickness control)	on sapphire: ultrathin polycrystalline or quasi-amorphous. At 250 °C, tens of nm of GaN show (002) polycrystalline formation with grain size < 10 nm ^[38] on glass: achieving pure GaN is difficult (O, H incorporation)	Angstrom-level thickness control, outstanding film uniformity, low-temperature capability allows application in postdevice processing, good for vertical-structure coating on glass Extremely slow growth rate, unsuitable for anything beyond thin films, limited precursor availability and high cost, lower crystal quality

The effect of the pretreatment can be verified by observing early GaN nucleation and buffer layer growth. For instance, when a nitridation step is applied to a glass surface, the initial GaN nuclei exhibit a lower density but grow larger in size with a dominant *c*-axis orientation. This occurs because the nitrogen species generated from nitridation are adsorbed onto the substrate and form strong bonds with the Ga atoms, leading to relatively large, well-aligned nuclei in the initial growth stage. In the absence of pretreatment, multiple nuclei randomly emerge, resulting in an

uneven grain size and poor orientation.^[40] In MOCVD processes, a two-step growth method is commonly used; a thin GaN or AlN buffer layer is first grown at a low temperature, followed by the main GaN layer grown at higher temperatures. This buffer layer strategy has been similarly applied to glass substrates.^[41] Some studies have also inserted an intermediate layer with good lattice compatibility, such as ZnO, before depositing GaN directly onto the glass to enhance the crystal quality.^[38] These buffer layers partially compensate for the lattice mismatch or manage the

thermal expansion differences between GaN and the underlying glass, thereby promoting uniform *c*-axis orientation and grain growth of the GaN film.^[35] GaN-on-glass films grown through proper pretreatment and buffer-layer incorporation tend to exhibit larger grains and improved crystallographic alignment; such microstructural improvements translate into enhanced optical and electrical properties.^[34]

The crystal quality of the GaN-on-glass thin films has been evaluated using various analytical methods. High-resolution XRD measurements of the FWHM of the rocking curve of (002) reflection have been used to determine the degree of mosaicity. For example, Chung et al. demonstrated that GaN grown on hexagonal boron nitride (*h*-BN) shows a (002) rocking curve FWHM of about 2.37°, indicating a relatively good vertical alignment. XRD ϕ -scans of the GaN (102) reflection are used to check the sixfold symmetry of wurtzite GaN crystals. Under proper conditions, GaN films grown on glass can also exhibit sixfold symmetry in the ϕ -scan, suggesting that, despite being polycrystalline, locally aligned domains predominate.^[42]

Electron backscatter diffraction (EBSD) is another powerful method for visualizing the orientations of individual grains. If the EBSD pattern shows that the GaN grains on glass mostly align their *c*-axis vertically and maintain consistent local orientations, then the material can be viewed as having a quasi-single-crystalline texture. Further insights into the optical quality can be obtained by measuring the band-edge emission intensity near 3.4 eV using photoluminescence (PL) spectroscopy and comparing it to any defect-related emission (e.g., yellow luminescence at \approx 2.2 eV). Generally, the higher the crystal quality, the stronger the band edge emission and the more suppressed the defect bands, which results in narrower emission linewidths.^[38] By integrating these techniques, including XRD rocking curves, ϕ -scans, EBSD, and PL measurements, the crystallographic quality of GaN-on-glass can be quantitatively assessed.

2.3.2. Methods for Improving GaN Crystallinity–Local Epitaxy

Researchers have introduced the concept of local epitaxy to enhance the quality of GaN films on glass substrates with inherently low crystallinity. While global epitaxy implies that the entire substrate surface grows with a single orientation on a nonlattice-matched substrate, such as glass, achieving uniform orientation across the entire substrate is practically not feasible. In contrast, local epitaxy focuses on inducing epitaxial growth within small localized domains that later merge to form quasi-epitaxial films.^[43] When GaN is grown directly on glass, numerous nuclei are formed in random orientations, resulting in a macroscopically polycrystalline film. Although local areas may exhibit epitaxial ordering, the overall film contains a mixture of differently oriented grains. With local epitaxy, the aim is to constrain each grain within a small region such that each grain can grow into a sizable domain before coalescing, effectively preventing large-area random orientations.^[41] Although the glass substrate does not provide directional information, local ordering followed by merging can significantly improve the crystallinity of the final GaN film. One method for realizing local epitaxy is to employ PA-MBE to spontaneously form GaN nanostructures. By tuning the N/Ga flux ratio during the MBE growth on glass, vertical GaN

nanowires or nanocolumns with diameters of tens of nanometers could be self-assembled.^[44] Individual nanowires act as discrete single crystals with low dislocation densities because they grow from the substrate without significant stress owing to lattice mismatch. However, the nanowires exhibit random positioning and anisotropic sidewall growth.

Another approach to local epitaxy is the use of SAG. This involves depositing a mask layer, such as SiO₂, SiN_x, or Ti, on the substrate surface and introducing lithographically defined stripes or micro-openings (holes) by etching certain regions so that GaN nuclei form only at predetermined locations.^[45,46] The mask suppresses peripheral growth and confines GaN to designated domains of a limited size. SAG-based epitaxial lateral overgrowth (ELOG) is widely used on sapphire substrate to reduce defect density and improve orientation. Extending the ELOG to glass, Wang et al. formed SiO₂ stripe masks on glass and induced lateral GaN overgrowth. Interestingly, unlike sapphire, the stripe orientation did not affect the overgrowth direction on glass, suggesting that the mask pattern itself guided the growth rather than any structural influence from the underlying substrate.^[41] This patterned growth leads to periodic uniform nanowires that avoid undesirable edge overgrowth. These approaches can be used for lateral merging to form a continuous film.^[47–52] This strategy is also applicable to amorphous glass substrates with a graphene preorienting layer and will be discussed in detail in Section 4.4.^[53] SAG and ELOG enable the formation of large coalesced grains with relatively flat surfaces, even on amorphous substrates, and are emerging as crucial technologies for large-area GaN-on-glass.

The GaN films supported by *c*-axis aligned nanowire template can be beneficial for optoelectronic devices. For instance, nanowire-based LEDs allow for uniform current distribution through each wire in a vertical path, and their sidewalls can serve as additional emission surfaces, boosting the light output. Moreover, cavities or photonic crystal structures leveraging nanowire arrays can further improve light-extraction efficiency, offering a new design of freedom. Hence, GaN nanowire arrays formed via local epitaxy can provide a strategy for GaN thin films and improving device performance in GaN-on-glass optoelectronics.

2.3.3. Methods for Improving GaN Crystallinity–2D Material Preorienting Layer

Another innovative strategy for improving the crystal quality of GaN grown on glass is the use of two-dimensional (2D) materials as intermediate layer. Graphene and *h*-BN are commonly investigated as 2D layered materials that can be applied to glass surfaces prior to GaN deposition.^[42] These 2D interfacial layers physically insert themselves between the glass and the GaN film, functioning as preorienting layers. Both graphene and *h*-BN are atomically flat and feature strong in-plane *sp*² bonding but weak bonding with the substrate, which can provide a partial lattice template at high temperatures. Notably, *h*-BN shares the same sixfold symmetry as GaN (unlike graphene) and can indirectly guide GaN orientation. As mentioned earlier, *h*-BN provides a clear sixfold symmetry to GaN, and EBSD shows a uniform *c*-axis orientation of GaN. These findings suggest that, even on amorphous substrates, a 2D layer can favorably align in the out-of-

plane direction (*c*-axis) and regulate the in-plane orientation of the GaN film to some extent.

Two mechanisms have been proposed to describe the GaN growth facilitated by 2D materials: quasi-van der Waals epitaxy (QvdWE) and remote epitaxy.^[54] QvdWE is not dependent on the crystallinity of substrate; it occurs even on amorphous materials. In this mechanism, the weak van der Waals interactions at the interface enable the deposited film to grow without being significantly affected by the lattice mismatch with the substrate.^[55] For example, when graphene is used as a 2D preorienting layer, defects or unsaturated carbon sites on its surface can locally induce chemical bonding between GaN nuclei and the graphene, promoting the formation of highly oriented nuclei. As these nuclei grow and coalesce, they may merge into a nearly single-crystalline film. In this context, QvdWE involves a mixed interfacial bonding regime in which weak van der Waals interactions coexist with a sparse covalent bonds—these localized bonds are critical for establishing an epitaxial relationship between the GaN film and the underlying graphene.^[56] In contrast, remote epitaxy becomes relevant when the base substrate is crystalline. Even when covered with an atomically thin 2D layer such as graphene, the electrostatic potential of the underlying lattice—arising from atomic charges or polarity—can partially transmit through the 2D layer. This enables the overlayer to “remotely” inherit the crystallographic orientation of the substrate. In remote epitaxy, there is no direct chemical bonding between the 2D interlayer and the growing films; instead, long-range electrostatic interactions such as Coulombic forces govern the alignment.

A long-standing debate centers on which mechanisms—QvdWE or remote epitaxy—is more favorable for the epitaxial growth of III-nitrides. Liu et al. provided key insights by investigating AlN growth on wet-transferred graphene.^[56] In their study, AlN films were grown on AlN/graphene substrates, enabling a direct comparison of remote epitaxy and QvdWE. It was found that remote epitaxy resulted in polycrystalline AlN films, whereas QvdWE consistently yielded single-crystalline AlN layers. In the case of remote epitaxy, the long-range electrostatic interaction from the AlN template was sufficient to suppress out-of-plane polarity inversion but failed to control in-plane alignment, leading to misoriented grains and ultimately polycrystallinity. In contrast, in QvdWE, localized chemical bonding at graphene defect sites anchored the in-plane lattice orientation of the initial nuclei, enabling coherent grain coalescence and the formation of continuous single-crystalline AlN or GaN film.

QvdWE is therefore considered more effective in achieving high-quality single-crystalline films. In contrast, pure van der Waals epitaxy (vdWE), which lacks any chemical bonding at the interface, has been reported to produce lower crystal quality due to poor control over initial nucleation. Indeed, studies have shown that III-nitride films grown via vdWE on pristine graphene often exhibit inferior crystallinity, attributed to the absence of robust nucleation sites. Nevertheless, remote epitaxy is not entirely ruled out. If the underlying substrate is a strongly polar single crystal, some lattice information can still be transmitted through the 2D layer. For example, in GaN-on-GaN remote epitaxy using graphene, the resulting GaN epilayers have been shown to retain the crystallographic orientation of the underlying substrate. However, unless the defect states of the graphene interlayer are precisely controlled, in-plane rotational disorder is difficult to suppress, leading

to grains with slight angular misalignment. This issue becomes particularly severe when the substrate is polycrystalline or amorphous, lacking a coherent lattice template.

In such cases, QvdWE becomes the dominant mechanism. When GaN is grown on an amorphous glass substrate, which lacks long-range order, 2D preorienting layers enable growth predominantly via QvdWE, resulting in a polycrystalline film with a preferred crystallographic texture. Although true single-crystal quality is not achieved, GaN-on-glass grown using 2D preorienting layers often exhibits a distinct sixfold symmetry in ϕ -scans and a relatively narrow (002) rocking curve FWHM, typically in the range of several hundred to a few thousand arcseconds—significantly better than what is observed for direct GaN growth on bare glass.^[42,57]

2.3.4. Challenges and Engineering Solutions in 2D-Assisted GaN Epitaxy

To employ 2D materials as preorienting layers on target substrates, it is common to use a transfer process in which 2D films synthesized via CVD are physically relocated onto the desired surface. However, this transfer step frequently introduces structural imperfections and mechanical damage to the 2D layer, significantly impacting the outcome of subsequent epitaxial growth. For example, CVD-grown graphene typically contains preexisting defects such as grain boundaries from and point defects, and further mechanical damage is often incurred during transfer. When polymer-supported layers (e.g., PMMA) are used to lift and relocate the graphene, incomplete adhesion to the substrate can lead to local tearing or cracking upon removal of the support. Wrinkles, tears, and pinholes commonly observed in transferred graphene films are generally attributed to such transfer-induced stresses.

Lee et al. reported that both intrinsic and handling-induced defects severely degrade the mechanical strength of CVD graphene, making it more susceptible to fracture and functional degradation.^[58] These damages compromise the structural continuity of the graphene layer and undermine its ability to withstand the high temperatures required for epitaxial growth. When the graphene is locally damaged, the underlying substrate may be exposed. If the exposed region is part of a single-crystal substrate, the resulting GaN nuclei may align with that crystal lattice, while nuclei forming on intact graphene evolve independently—leading to nonuniform orientation. On polycrystalline substrates, exposed regions may vary in crystallographic orientation, further increasing the likelihood of grain misalignment in the overgrown GaN. Moreover, lateral overgrowth of GaN onto exposed substrate regions disrupts the intended epitaxial interface, exacerbating lattice mismatch and introducing grain boundaries. These observations highlight the critical importance of maintaining the structural integrity of the graphene interlayer.

GaN epitaxy typically requires high temperatures ($\approx 1000^\circ\text{C}$), making the thermal stability of the interfacial 2D material a key consideration. Graphene, in particular, is vulnerable to decomposition or sublimation at elevated temperatures. Park et al. found that graphene's thermal stability is highly dependent on the underlying substrate.^[59] For instance, graphene was partially preserved after annealing above 1300°C on sapphire, which contains oxygen,

whereas it completely degraded under similar conditions on AlN, which contains nitrogen. This degradation was attributed to nitrogen species released from AlN decomposition at high temperatures, which chemically attack the graphene layer.

In contrast, *h*-BN remained structurally intact under the same condition. Although it shares a similar hexagonal lattice structure with graphene, *h*-BN's alternating boron and nitrogen atoms confer enhanced chemical stability in nitride-rich environments. In the same study, *h*-BN was used as an interfacial layer on AlN templates for AlN thin film growth. After growth, the *h*-BN layer remained intact and enabled clean exfoliation of the overgrown film, showing the importance of thermal stability for 2D interlayers in high-temperature processes such as MOCVD or HVPE. When using monolayer graphene, growth conditions must be carefully optimized to preserve its interfacial function. A well-known consequence of thermal instability is degradation in crystallinity or even complete failure of epitaxy. Kwak et al. demonstrated this during MOCVD growth of GaN on graphene/AlN templates.^[60] While initial nucleation at 750 °C enabled exfoliation, subsequent growth at 1050 °C caused graphene degradation near surface pits on the AlN. As a result, GaN began to grow directly on the exposed AlN, resulting the overgrown film nonexfoliable.

To overcome such limitations, the use of multilayer 2D materials has emerged as a promising strategy. "Multilayer" here refers to both vertical stacking of identical 2D layers (e.g., bilayer or trilayer graphene) and the integration of heterogeneous materials. This approach serves two primary functions. First, monolayer graphene is highly susceptible to pinholes; even a single defect can result in direct substrate expose. By stacking multiple layers, the probability of pinholes aligning across all layers decreases significantly, providing a more continuous barrier that better isolates the substrate. Each layer can compensate for defects in others. Bilayer and trilayer graphene have been shown to reduce crack formation from transfer-induced stress and better accommodate thermal expansion mismatches. However, excessively thick stacks may fully screen lattice-level interactions, making orientation control of GaN nuclei difficult.^[56] Therefore, when using multilayer graphene, the growth mechanism is more likely to follow QvdWE, where the primary function of the interlayer is to ensure a defect-free interface. Another strategy involves heterogeneous stacking, such as bilayer of graphene and *h*-BN. Graphene provides excellent thermal conductivity and mechanical strength, while *h*-BN offers superior thermal and chemical stability. For example, *h*-BN can maintain its structural role throughout high-temperature GaN growth, preserving interfacial integrity.^[59] This hybrid configuration leverages the strengths of each material: *h*-BN for stability, graphene for exfoliability and thermal transport.

A second key strategy involves precise control of the growth process. Ensuring a defect-free, conformal transfer of the 2D interlayer is essential. Transfer techniques such as soft polymer-supported transfer, roll-to-roll lamination, or optimized wet etching should be fine-tuned to minimize wrinkles and ensure uniform adhesion. Post-transfer annealing must also be optimized to remove polymers residues without damaging the 2D material.^[58] During growth, process conditions must suppress thermal degradation and avoid unintended chemical reactions. For example, Kwak et al. used a two-step MOCVD process:

GaN nucleation began at 750 °C, followed by high-temperature growth at 1050 °C to promote coalescence, with the goal of protecting the graphene layer.^[60] Although surface pits still caused partial degradation, the approach demonstrated the value of thermal step control. Critical parameters such as ramping rate, precursor injection timing, and NH₃/H₂ flow ratios must be carefully managed to preserve interfacial stability.

To promote QvdWE and induce in-plane alignment, it is also important to control the density and type of interfacial defects. Too few defects may lead to random nucleation; too many can compromise the graphene's continuity or lead to excessive nucleation density and polycrystallinity. Liu et al. addressed this by exposing graphene to atomic nitrogen plasma to introduce C–N dangling bonds—defects sites that serve as moderate nucleation anchors.^[56] By optimizing plasma exposure time and integrity, they maintained graphene's structure while introducing sufficient nucleation sites to achieve single-crystalline GaN films. Finally, substrate surface preparation is critical. The substrate must be atomically clean and flat to ensure uniform adhesion of the 2D interlayer. Pregrowth treatments should remove surface roughness and residual reactive species that may cause local breakdown or nonuniform bonding under thermal stress. In summary, the successful use of 2D materials in III-nitride epitaxy requires comprehensive optimization—from substrate preparation to interlayer transfer, defect engineering, and thermal process control. Only by addressing each stage meticulously can the full potential of 2D-assisted GaN-on-glass integration be realized.

2.3.5. Polarity Control and Transmission in GaN Growth on 2D Preorienting Layer

As discussed in the previous section, introducing a 2D preorienting layer serves as an effective strategy for improving the crystallinity of heteroepitaxial GaN by mitigating lattice mismatch constraints. Another critical parameter in GaN epitaxy is the ability to control and maintain the lattice polarity of the epilayer. GaN crystallizes in a noncentrosymmetric wurtzite structure and exhibits strong spontaneous polarization along the *c*-axis, leading to two distinct polarities: Ga-polar ((0001) orientation) and N-polar ((000-1) orientation), depending on whether Ga or N atoms terminate the top surface.^[61] Polarity profoundly affects surface chemistry, electrical behavior, and defect formation in the epitaxial layer, making precise polarity control essential for device applications such as LEDs and lasers. The polarity of GaN is primarily determined during the initial nucleation and is dictated by the atomic configuration and chemical bonding at the interface. The atom that first bonds with the substrate during nucleation generally determines the resulting polarity. For instance, inserting a low-temperature AlN buffer layer between GaN and a sapphire substrate allows Ga atoms to preferentially bond with the buffer, promoting Ga-polar GaN growth. In contrast, direct growth without a buffer often results in N-polar GaN, as N atoms bond with the substrate surface.^[62] Polarity can also be tuned by adjusting surface treatments and initial growth parameters, such as the III/V precursor ratio and temperature, even when using the same substrate, highlighting the sensitive Ga–N bond orientation to the growth environment.^[63] In general, if Ga atoms bond at the interface with N atoms positioned above,

the resulting film exhibits N-polarity; conversely, if N atoms bond at the interface and Ga atoms grow on top, Ga-polarity is favored. Once established, this polarity tends to propagate vertically through the film due to the energetic stability of the initial bonding configuration. Reversing polarity mid-growth requires forming high-energy inversion domain boundaries or dislocations, which is energetically unfavorable. Therefore, the initial polarity typically persists throughout the entire film thickness. However, if nuclei with mixed polarity form during nucleation, inversion domains may arise, increasing defect density and degrading both optical and electrical performance. Thus, achieving uniform polarity is critical.

Epitaxy on 2D materials such as graphene or *h*-BN introduces new challenges and strategies for polarity control. Unlike conventional substrates, 2D materials do not provide strong interfacial chemical bonding, making GaN nucleation more prone to mixed polarity. For example, monolayer graphene is chemically inert and does not preferentially bond with either Ga or N atoms, increasing the likelihood of random polarity nucleation or even suppressed nucleation. Part et al. demonstrated that although *h*-BN can act as a favorable template for initiating GaN epitaxy, graphene presents notable difficulties in achieving consistent crystallization.^[64] Consequently, establishing polarity-controlled GaN films on 2D layers requires deliberate engineering of polarity-selective interfacial bonding. One approach involves chemically functionalizing the 2D layer to introduce favorable nucleation sites. In the case of graphene, this may include doping with heteroatoms or introducing surface defects to guide polarity selection. Liu et al. showed that the polarity of GaN grown on O-doped graphene can be switched depending on the order of precursor supply: supplying Ga first results in N-polar films, whereas supplying N first yields Ga-polar films.^[65] This dual-mode selectivity is a significant demonstration that interfacial atomic configuration can be harnessed to control GaN polarity on 2D materials.

Beyond graphene, *h*-BN has also been explored as a preorienting layer for polarity control. Unlike graphene, *h*-BN exhibits intrinsic polarity, with one surface terminated by B atoms and the other by N atoms. When transferred onto a substrate, *h*-BN can either shield the substrate's electrostatic potential or strongly bond with it, depending on its orientation and defect density.^[66] For example, Kong et al. reported that monolayer *h*-BN bonded strongly to GaN substrates, effectively blocking remote epitaxial interactions.^[55] Introducing defects into *h*-BN allowed partial transmission of the substrate's potential, enabling epitaxial alignment. These results indicate that chemical state of the *h*-BN interface can influence both the orientation and polarity of the overgrown GaN layer. However, unlike graphene, strategies for chemically tuning *h*-BN polarity via doping remain largely unexplored.

In summary, polarity in GaN epitaxy on 2D materials is governed by the atomic bonding configuration at the nucleation interface. Controlling this requires precise engineering of the interfacial chemistry—via doping, defect engineering, or precursor sequencing—and precise control of early-stage growth conditions. The ability to manipulate polarity on 2D materials not only deepens our understanding of QvdWE or remote epitaxy but also expands the design flexibility of GaN-based heterojunction devices beyond conventional substrate limitations. These strategies

are expected to extend to other polar III-nitrides, such as AlN and InN, and contribute to new frontiers in epitaxial crystal growth and device integration.

3. GaN Thin Film on Bare Glass Substrates

The direct growth of GaN thin films on amorphous glass substrates presents significant challenges owing to the lack of a lattice structure, which leads to polycrystalline GaN formations despite the initial appearance of uniform growth. Sections 3.1 and 3.2 provide an in-depth examination of these challenges, beginning with the baseline growth characteristics of GaN on bare glass (Section 3.1) and advancing controlled growth techniques (Section 3.2) aimed at providing in-plane symmetry and structural quality. Strategies, such as SAG using Si₃N₄ stripe patterns and nanoimprint lithography, have been employed to restrict the growth planes and promote 1D columnar coalescence, thereby enabling the subsequent fabrication of SiO₂ mask holes for the growth of GaN nanorods on amorphous glass. These approaches have demonstrated significant progress in achieving *c*-axis-oriented growth but also highlight the persistent challenges of attaining in-plane symmetry, indicating the critical influence of the amorphous substrate. This section explores the growth mechanisms and fundamental limitations imposed by the amorphous nature of the substrate, thereby providing valuable insights into the epitaxial growth of GaN on amorphous glass.

3.1. Growth of GaN Thin Film on Bare Glass

Figure 1a shows three schematic representations of GaN growth: local epitaxy, global epitaxy, and absence of epitaxy.^[67] The concept of local epitaxy refers to the preferred growth direction along *z*-direction (*c*-axis) toward the surface normal, whereas the *a*-axes are randomly oriented in the *xy*-plane. Because GaN growth occurs on a polycrystalline preorienting layer, the resulting GaN exhibits a polycrystalline nature. Global epitaxy, in contrast, involves growth on a single-crystalline substrate in which both the *c*-axis and *a*-axis of GaN are fully coherent with the substrate lattice. Further, the absence of epitaxy results in completely random orientation of both the *c*-axis and *a*-axis. However, when considering GaN growth on amorphous glass using various epitaxial techniques, the *c*-axis orientation is preferred. The highest surface energy along the (002) orientation results in the highest growth rate, leading to the *c*-axis orientation.^[38,68,69]

Figure 1b,c shows planar and cross-sectional scanning electron microscopy (SEM) images of polycrystalline GaN grown by electron cyclotron resonance (ECR)-MBE on a nitridated glass substrate.^[40] Highly oriented, coalescent, and columnar GaN structures with smooth morphologies are visible. The inset of the streaky reflection high-energy electron diffraction (RHEED) pattern confirms a smooth morphology. However, no changes are observed in the two types of diffraction patterns during rotation, indicating that the *c*-axis-oriented polycrystalline GaN is randomly oriented along the *a*-axis. Figure 1d shows a cross-sectional transmission electron microscopy (TEM) image of polycrystalline GaN at the GaN/glass interface, projected along the (11–20) direction. The measurements confirm columnar growth along the (002) direction, with a mean grain size ranging from 30 to 50 nm.^[70]

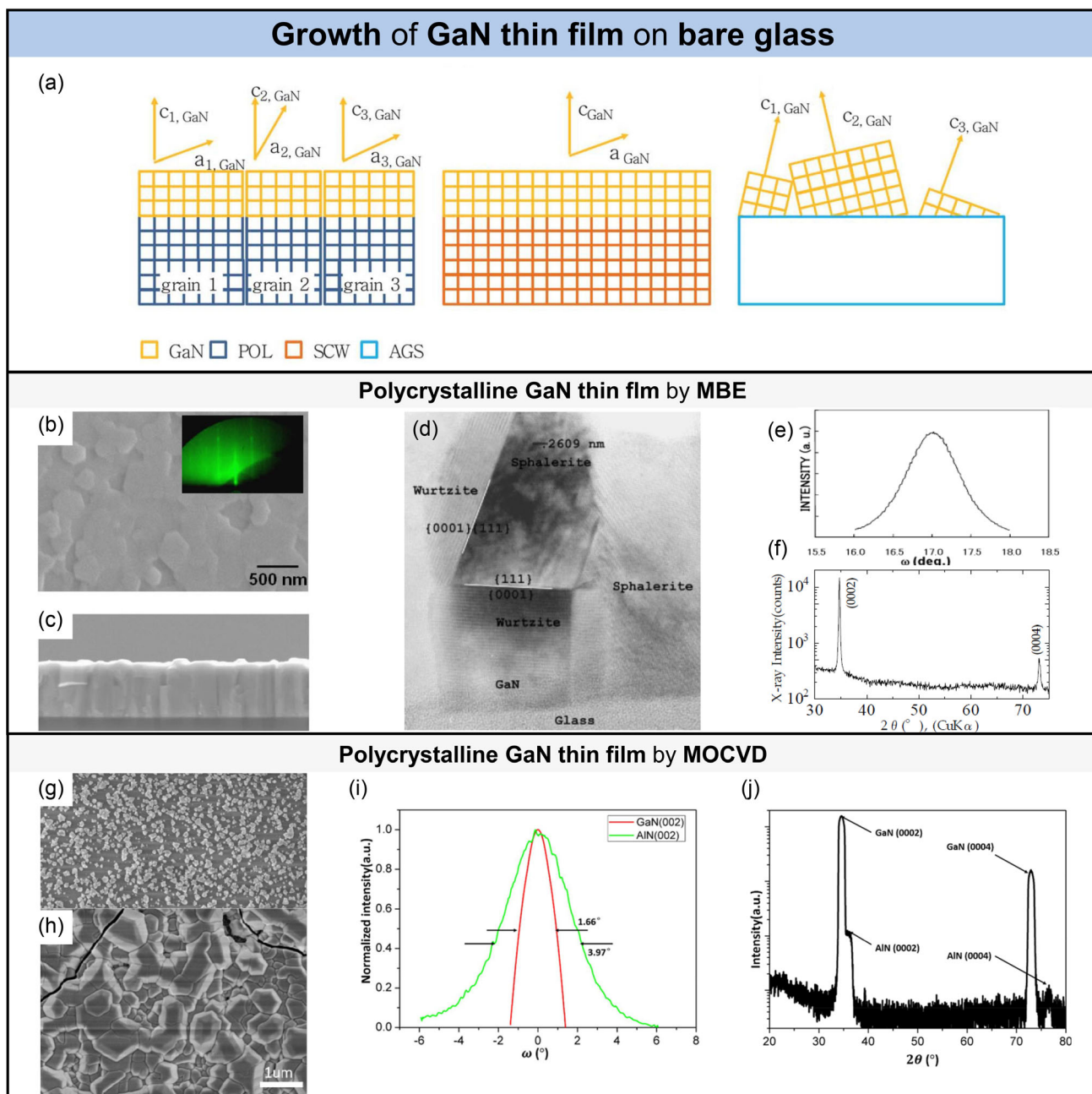


Figure 1. a) Schematic representation of local epitaxy, global epitaxy, and the absence of epitaxy. In both local epitaxy and global epitaxy, the c -axis of GaN is directed along the z -direction, while the a -axis lies in the xy -plane. In contrast, the c -axis and a -axis of GaN are randomly oriented in the absence of epitaxy. POL, SCW, and AGS represent the preorienting layer, single-crystal substrate, and amorphous glass substrate, respectively. Reproduced with permission.^[67] Copyright 2012, Royal Society of Chemistry. b) Planar and c) cross-sectional SEM images of the polycrystalline GaN thin film grown on a nitridated glass substrate. The inset in (b) shows the spot-streak RHEED, indicating that the c -axis of GaN is uniformly oriented. Reproduced with permission.^[40] Copyright 2003, Wiley-VCH. d) Cross-sectional TEM image of polycrystalline GaN, projection along the (11-20), with the formation of hexagonal and cubic GaN. Reproduced with permission.^[70] Copyright 2003, Wiley-VCH. e) XRD (002) rocking curve of polycrystalline GaN on a glass substrate which indicating a value of less than 1° . Reproduced with permission.^[40] Copyright 2003, Wiley-VCH. f) XRD 2θ -scan measurement results of polycrystalline GaN on a glass substrate showing hexagonal wurtzite-type GaN. Reproduced with permission.^[71] Copyright 2017, Wiley-VCH. Planar SEM images of the polycrystalline thin film GaN on g) bare glass and h) AlN/glass substrates. i) XRD (002) rocking curve of polycrystalline GaN (red solid line: 1.66°) on an AlN/glass substrate and AlN (green solid line: 3.97°), respectively. j) XRD 2θ -scan measurement results of polycrystalline GaN on an AlN/glass substrate. Reproduced with permission.^[68] Copyright 2015, Wiley-VCH.

Various crystal phases, including sphalerite, cubic, and wurtzite hexagonal phases, are observed along with several defects such as basal stacking faults and inversion domain boundaries. The sample exhibits a (002) XRD rocking curve with an FWHM of less than 1° (Figure 1e). Despite the multiple crystal phases at the GaN/glass interface, the XRD 2θ -scan measurement reveals that polycrystalline GaN-on-glass predominantly exhibits a hexagonal wurtzite-type GaN crystal phase, as shown in Figure 1f.^[71]

Subsequently, An et al. grew a GaN thin film on an RF-sputtering-deposited AlN/glass substrate using MOCVD and compared the results.^[68] Similar to GaN grown on bare glass using ECR-MBE, small columnar GaN grains were observed on the bare glass because of the large nucleation energy of GaN (Figure 1g).^[72] In contrast, the MOCVD-grown GaN layer on the RF-sputtering-deposited AlN/glass substrate exhibited an improved morphology, as shown in Figure 1h. However, the GaN grains on the AlN buffer layer did not fully merge into a continuous thin film because of the random in-plane orientation. Figure 1i,j shows that the *c*-axis is still not completely oriented, even with the use of the AlN buffer layer (XRD rocking curve with an FWHM of 1.6°), although the hexagonal wurtzite structures of GaN and AlN are maintained.

3.2. Controlled Growth of Thin Film GaN on Bare Glass

As previously discussed, polycrystalline GaN grown on bare glass using ECR-MBE demonstrated that a coalescent columnar GaN structure improved the surface uniformity of the thin film while maintaining small grain sizes. Another promising method for achieving such structural growth is PA-MBE, which produces submicron-scale polycrystalline grains of highly *c*-plane-oriented GaN on amorphous glass substrates at low growth temperatures.^[73] Under the Volmer–Weber (VW) growth mode and nitrogen-rich conditions with a high V/III flux ratio, coalesced GaN columns can form preorienting layers, enhancing the uniformity.^[45,69,74] Additionally, the predominance of N-polarity, achieved without the use of an Al platform, can lead to significant changes in the energy band profiles of heterojunctions.^[75] This feature enables various electronic and optoelectronic applications, such as field-effect transistors (FETs) utilizing two-dimensional electron gases at the GaN/AlGaIn interface,^[76] highly efficient LEDs with enhanced indium incorporation and external quantum efficiency (EQE),^[77,78] and other advanced devices.

During the growth of polycrystalline GaN layers via PA-MBE, an intermediate Si_3N_4 layer was employed because of its thermal expansion coefficient, which lies between those of GaN and glass. This effectively reduces the detrimental stress on the GaN layer during cooling. Furthermore, Si_3N_4 can be easily deposited onto thermally durable substrates. **Figure 2a** presents a schematic and tilted-view SEM image of coalescent columnar GaN grown on a glass substrate using PA-MBE.^[79] Each grain exhibits a diameter of ≈ 100 nm on surface of the coalescent columnar GaN, with the *c*-plane growth direction oriented perpendicular to the glass surface. The inset shows the discrete RHEED patterns of the (002), (004), (101), and (103) orientations with fixed pattern positions during rotation, indicating the absence of a preferential direction for the *a*-axis of GaN.^[80] Additionally, several cracks can be

observed on the coalescent columnar GaN surface, which is attributed to the difference in the thermal expansion coefficient between GaN and glass. Figure 2b,c presents schematics and tilted-view SEM images of MOCVD-grown planar GaN and GaN grown using the SAG method for 15 min, respectively. The schematics illustrate the growth mode transitions from VW to Stranski–Krastanov (SK) during MOCVD growth, resulting in the formation of GaN micrograins. In the MOCVD-grown planar GaN (Figure 2b), each grain exhibits varying sizes and angles between adjacent grains. However, in the MOCVD-grown GaN using the SAG method (Figure 2c), SiO_2 stripe-patterned masks are employed to mitigate irregular coalescence with neighboring grains. This approach effectively reduces the number of degree of freedom in the in-plane growth direction by half. Consequently, the morphology shows regularly aligned GaN micrograins along the mask patterns, demonstrating that the morphology of MOCVD-grown GaN can be precisely controlled using the SAG method.^[81] The size of the platelet-shaped GaN grains produced by the SAG method is approximately twice that of planar GaN. The cracks observed in the PA-MBE-grown coalescent columnar GaN are covered by coalescence above the crack boundaries (Figure 2d). Further growth promotes lateral overgrowth, filling the gaps between the GaN micrograins. However, the structure still displays a distorted 3D microstructure owing to the absence of in-plane symmetry (Figure 2e).

To further restrict the degrees of freedom in nitrogen-polar coalescent columnar GaN/glass, holes were created on the SiO_2 mask using a nanoimprint process. Subsequently, the MOCVD GaN grew within these holes, resulting in the formation of GaN nanorods.^[82] Figure 2f shows the LED mesa pattern of the GaN nanorod arrays grown by MOCVD, along the tilted-view SEM images of the morphology of the GaN and InGaIn/GaN core-shell nanorods. The densely packed nanorods were fully elongated and exhibited flat-top shapes, which is a characteristic feature of nitrogen polarity. The detailed procedure for fabricating the SiO_2 hole mask pattern via nanoimprint lithography is presented in Figure 2g. As shown in Figure 2h, the out-of-plane and in-plane symmetries of the coalescent columnar GaN grown on glass via PA-MBE and the GaN nanorods grown using the SAG method with MOCVD were measured using EBSD. Both samples showed a preferential orientation along the (002) direction. However, in the (10–12) plane, both samples exhibited dispersed circular ring patterns, indicating the absence of a preferential direction along the *a*-axis of GaN. Although each GaN nanorod retained sixfold symmetry, the overall GaN nanorod ensemble still lacked in-plane symmetry. Nevertheless, localized spots are observed in the figures, which can be attributed to the low sampling numbers caused by the enlarged size of the GaN nanorods and the shadowing effect of the 3D structures. The nanorod growth method using SAG demonstrated that epitaxial growth could be achieved even on templates with thin and weak crystalline quality on amorphous glass. Bae et al. successfully demonstrated GaN nanorods and InGaIn/GaN core-shell structures on amorphous glass substrates and analyzed their structural and optical properties, which showed promising potential for device applications.^[82]

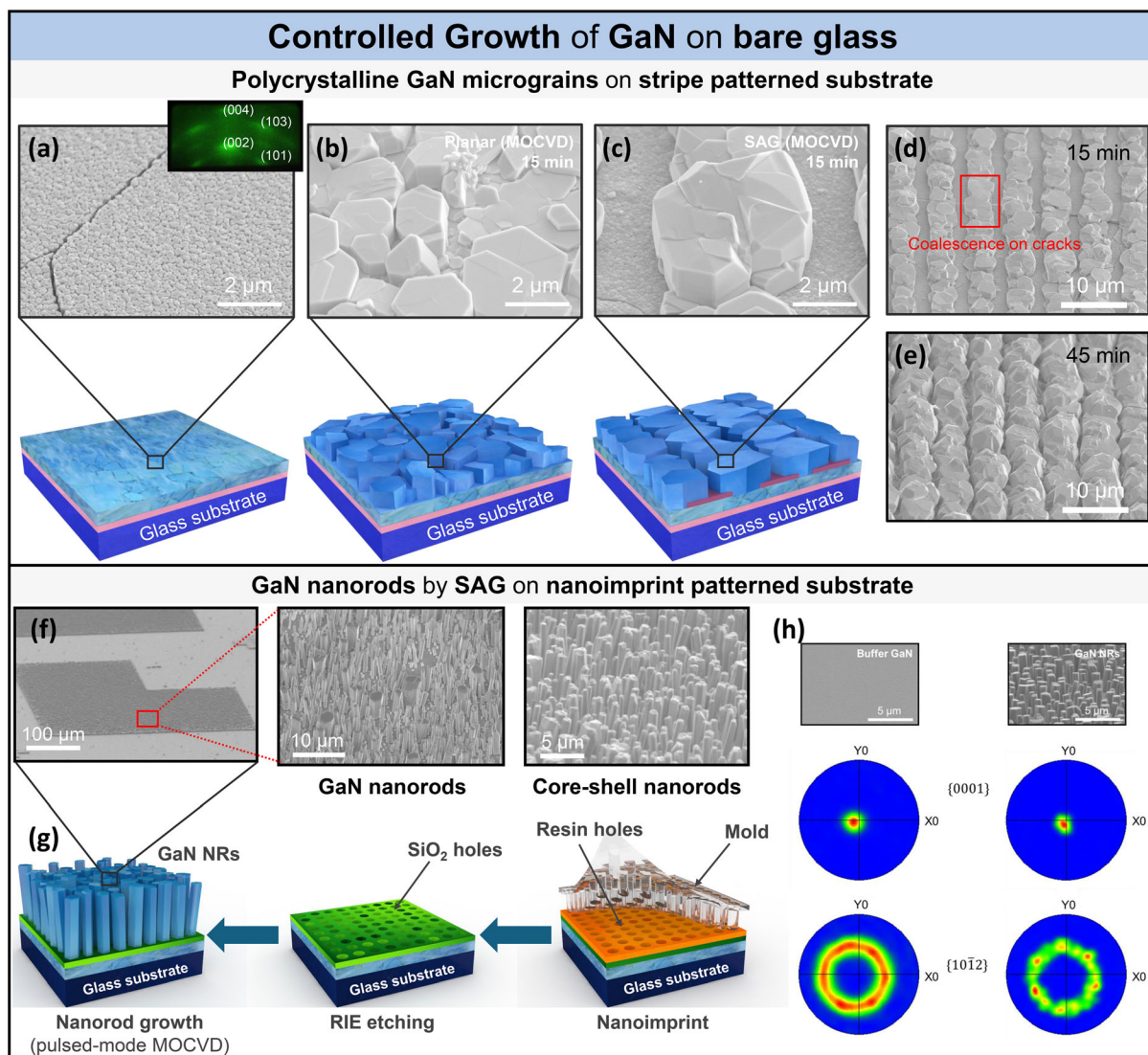


Figure 2. Schematic representation and corresponding tiled-view SEM images of a) PA-MBE-grown coalesced columnar GaN on an $\text{Si}_3\text{N}_4/\text{glass}$ substrate, b) MOCVD-regrown GaN on coalesced columnar GaN, and c) MOCVD-regrown GaN using the SAG method on coalesced columnar GaN with SiO_2 stripe-patterned masks. Reproduced with permission.^[79] Copyright 2016, IOP Publishing Ltd. SEM tilted views of MOCVD-regrown GaN using the SAG method for d) 15 min and e) 45 min, respectively. Reproduced with permission.^[81] Copyright 2015, Royal Society of Chemistry. f) SEM tiled view of MOCVD-regrown GaN nanorods using the SAG method on coalesced columnar GaN with nanoimprinted masks. GaN nanorods were grown over a large area, with higher magnification revealing densely packed, elongated GaN nanorods. InGaN/GaN core-shell nanorods are also shown on the right. g) Schematic representation of the growth procedures for MOCVD-regrown GaN nanorods using the SAG method on coalesced columnar GaN with nanoimprinted masks. EBSD results of h) coalesced columnar GaN and GaN nanorods, respectively. Reproduced with permission.^[82] Copyright 2017, Nature Portfolio.

4. GaN on Preorienting Layer-Coated Glass Substrates

In this section, GaN nanostructures and thin films grown on preorienting layer-coated glass substrates are discussed for their applications in optoelectronic devices. Building on the concepts of local and global epitaxy introduced in the previous section, this study expands the discussion on preorienting layers to include more comprehensive approaches. For instance, thermally stable and highly conductive thin films, such as Ti or Ti_3C_2 MXene, can

be used as preorienting layers to enhance the crystallinity of nanostructures while providing sufficient electrical conductivity for device operation. Alternatively, GaN nanostructures can be grown on indium tin oxide (ITO)-coated glass, which offers both transparency and conductivity, enabling heterogeneous integration with other materials. The vapor-liquid-solid (VLS) method is also a promising approach for device implementation. GaN nanostructure arrays exhibit hexagonal symmetry in individual nanostructures along the in-plane direction, although the overall ensemble lacked in-plane symmetry. Despite these limitations,

these structures demonstrate the feasibility of fabricating functional optoelectronic devices on amorphous substrates.

Approaches using GaN thin films on amorphous substrates leverage 2D materials as preorienting layers. **Table 3** summarizes recent studies in which single-crystalline GaN was successfully grown on amorphous substrates using various 2D materials, such as graphene, WS₂, *h*-BN, and MoN, as preorienting layer. These examples highlight the role of 2D materials in promoting epitaxial alignment and improving crystalline quality, even in the absence of long-range order in the underlying substrate. Unlike nanostructures, thin films form uniform layers during merging, thereby exhibiting in-plane symmetry. An additional advantage of 2D materials is their weak bonding at the 2D material interface, which enables the exfoliation of thin films. The strategies discussed in this section are expected to significantly enhance the performance and potential of GaN-based devices on amorphous glass substrates, thereby paving the way for innovative advancements in optoelectronics.

4.1. Growth of GaN Nanostructures on Preorienting Layer

ITO has achieved significant industrial success and is widely used as a current-spreading layer in LEDs^[83,84] and as a transparent conductive layer (TCL) in perovskite solar cells (PSCs).^[85] GaN-based devices in industry are primarily grown using MOCVD, which relies on high-temperature processes, making

GaN growth on ITO impractical. However, using PVD methods, GaN growth on ITO is feasible at low temperatures.^[86,87] Inspired by this, Prabaswara et al. demonstrated the direct growth of GaN nanowires on ITO-coated glass using PA-MBE.^[88] A 100-nm-thick ITO layer was deposited onto an amorphous glass substrate via RF magnetron sputtering, followed by rapid thermal annealing (RTA) at 650 °C. **Figure 3a** shows a schematic of the columnar ITO grains formed after RTA. Subsequently, GaN nanowires were grown in a nitrogen-rich environment, on top of the ITO grains. The nanowires were analyzed using high-annular dark-field scanning transmission electron microscopy (HAADF-STEM), which confirmed the successful growth of GaN on the ITO surface (**Figure 3b**). As shown in **Figure 3c**, the GaN nanowires showed nitrogen polarity, and the GaN/ITO interface revealed a nonuniform region of ≈ 4 nm thickness, where polycrystalline and amorphous phases coexisted (**Figure 3d**).

No clear epitaxial relationship was observed between the ITO and GaN nanowires. However, the growth of GaN on 2D materials presents a promising opportunity for advancing the epitaxial growth of GaN on amorphous substrates. Prabaswara et al. demonstrated the epitaxial growth of GaN nanowires on Ti₃C₂ MXene nanoflake films using PA-MBE and investigated their properties.^[89] MXene is a promising preorienting layer for glass substrates because of its high thermal stability, high metallic conductivity ($0.5\text{--}8\text{ k}\Omega\text{ sq}^{-1}$), and partial transparency (40%–90%),^[90,91] making it highly suitable for device applications. **Figure 3e** shows a schematic of GaN nanowires grown on Ti₃C₂ MXene nanoflakes. The Ti₃C₂ MXene

Table 3. The progress of 2D material-assisted single-crystal GaN film epitaxy on amorphous substrates.

Institution (year)	GaN crystallinity	Epi structure	Preorienting layer	Growth template	Growth method
Seoul National Univ. (2012) ^[98]	<i>c</i> -plane orientation with twelve-fold symmetry	Blue LED on ZnO nanowalls buffer layer	Graphene	Glass	MOCVD
Univ. of Tokyo (2014) ^[57]	<i>c</i> -plane orientation with sixfold symmetry	Blue LED on AlN buffer layer	Graphene	Glass	PSD
Univ. of Tokyo (2014) ^[95]	<i>c</i> -plane orientation with sixfold symmetry	GaN thin film	Graphene	100-nm-thick SiO ₂ on Si(100)	PSD
Seoul National Univ. (2017) ^[42]	<i>c</i> -plane orientation with sixfold symmetry	GaN thin film	<i>h</i> -BN	Glass	MOCVD
Taiyuan Univ. of Tech. (2018) ^[123]	<i>c</i> -plane orientation	GaN thin film	Graphene	300-nm-thick SiO ₂ on Si	MOCVD
Tsinghua Univ. (2019) ^[124]	<i>c</i> -plane orientation with sixfold symmetry	GaN thin film on AlN buffer layer	Graphene	Copper sheet	PA-MBE
National Research Nuclear University MEPhI (2019) ^[125]	<i>c</i> -plane orientation with sixfold symmetry	GaN thin film on AlN buffer layer	Graphene	300-nm-thick SiO ₂ on Si	PA-MBE
Chinese Academy of Sciences (2021) ^[53]	<i>c</i> -plane orientation with sixfold symmetry	Blue LED on coalescence layer of AlGaIn nanorods	Graphene	Glass	MOCVD
Chinese Academy of Sciences (2022) ^[97]	<i>c</i> -plane orientation with sixfold symmetry	Blue LED on AlGaIn buffer layer	WS ₂	Glass	MOCVD
KAUST (2022) ^[96]	<i>c</i> -plane orientation with sixfold symmetry	GaN thin film	MoN	Glass	PA-MBE
Chinese Academy of Sciences (2023) ^[126]	<i>c</i> -plane orientation with sixfold symmetry	GaN thin film on AlGaIn buffer layer	WS ₂	Glass	MOCVD
Chinese Academy of Sciences (2024) ^[111]	<i>c</i> -plane orientation with sixfold symmetry	Blue LED and PD on AlN buffer layer	Graphene	400-nm-thick SiO ₂ on Si(100)	MOCVD

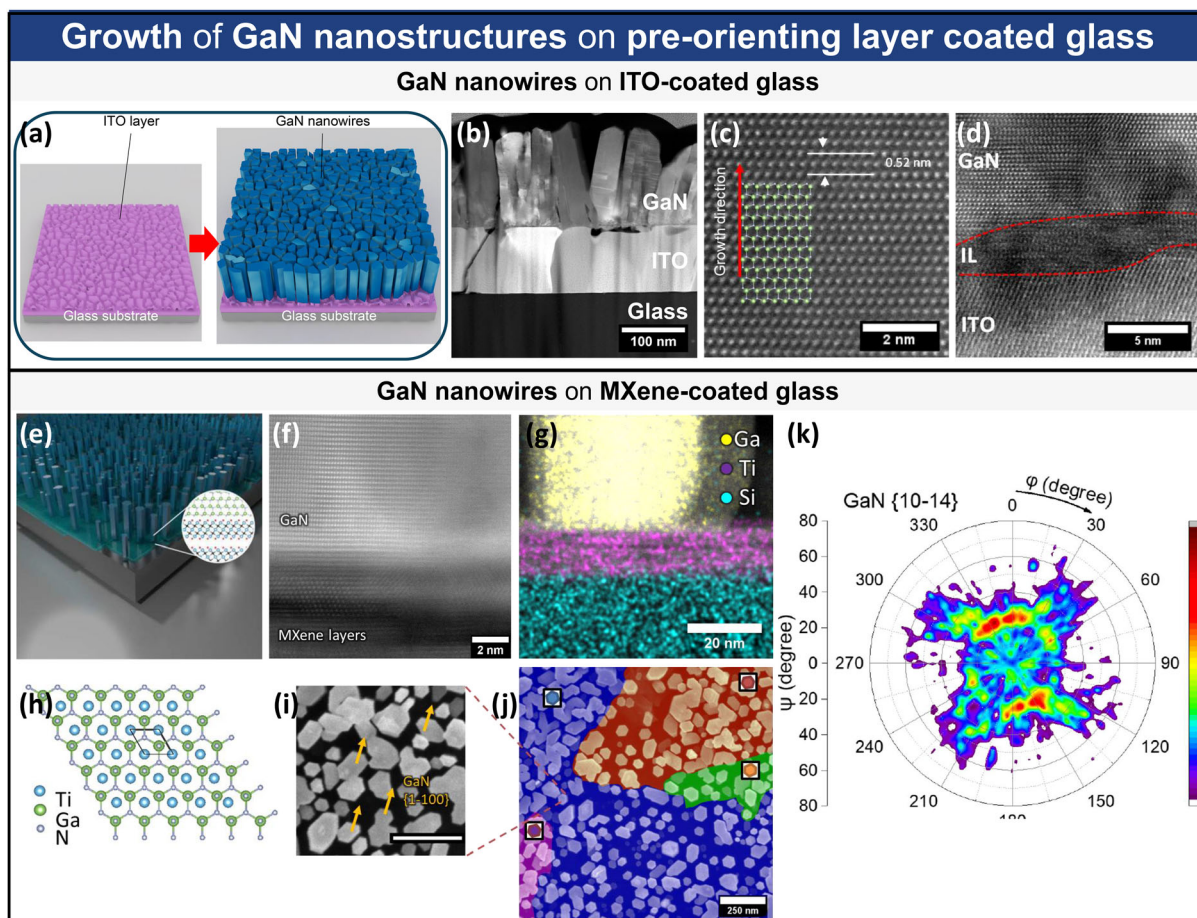


Figure 3. a) Schematic representation of GaN nanowires grown on an ITO-coated glass substrate. b) Cross-sectional TEM image of GaN nanowires on an ITO-coated glass substrate. c) High-resolution TEM image of GaN nanowires, indicating the single-crystalline nature of GaN. The red solid arrow shows the growth direction of the *c*-axis GaN. d) High-resolution cross-sectional TEM image of the interface between GaN and ITO. Reproduced with permission.^[188] Copyright 2019, Springer. e) Schematic representation of GaN nanowires grown on an MXene-coated glass substrate. f) High-resolution cross-sectional TEM image of the interface between GaN and MXene. g) EDS elemental mapping image at the GaN/MXene interface. h) Schematic image of the atomic configuration between the first atomic plane of hexagonal wurtzite GaN and Ti_3C_2 MXene. i) Planar SEM image of GaN nanowires grown on an MXene-coated glass substrate, with the yellow solid arrow indicating identical in-plane orientation of GaN. j) False-color mapping of the planar SEM image of GaN nanowires on MXene, where each color represents a distinct in-plane direction of GaN. k) XRD pole figure of GaN nanowires on MXene, showing a random in-plane orientation distribution of GaN. Reproduced with permission.^[189] Copyright 2020, American Chemical Society.

solution was spray-coated onto a glass substrate using an air-brush, and the thickness was controlled by adjusting the coating time. Figure 3f shows a high-resolution HAADF-STEM image of the GaN/MXene interface, revealing the lattice structure of GaN grown directly on the MXene film along the *c*-plane direction. Energy-dispersive X-ray elemental mapping (Figure 3c) confirmed that Ga, Ti, and Si formed distinct interfaces without diffusion across the boundaries. As shown in Figure 3h, the primitive unit cell distance of GaN in the (11-20) direction is 3.189 \AA , whereas Ti has a similar distance of $\approx 3.071 \text{ \AA}$ in the same direction, resulting in a lattice mismatch of $\approx 3.7\%$. This small lattice mismatch supports the potential of MXene as a preorienting layer for high-quality GaN growth. SEM measurement was conducted to confirm the in-plane epitaxial relationship of GaN grown on MXene. Figure 3i shows a high-magnification planar SEM image of the GaN nanowires, clearly revealing that the hexagonal

nanowires were aligned in specific directions within the in-plane orientation. To further validate this observation, a low-magnification planar SEM image was obtained (Figure 3j). As is evident from the false-colored images, distinct in-plane orientations can be identified within small regions. The presence of multiple in-plane orientations indicates an epitaxial relationship between the GaN nanowires and MXene nanoflakes. However, the XRD pole figure measured in the GaN (10–14) direction shows a lack of symmetry over a wide range, suggesting that the MXene nanoflakes coated on an amorphous substrate cannot fully transfer in-plane symmetry to GaN (Figure 3k). Nevertheless, these measurements strongly suggest that if a few monolayers of a 2D material are uniformly coated onto the substrate, then they can provide extensive in-plane symmetry to GaN. This feature highlights the potential of 2D materials for achieving uniform epitaxial growth and GaN-based technologies.

4.2. GaN Nanostructures on Glass: Device Applications

In local epitaxy, epitaxial growth occurs on a polycrystalline preorienting layer. Although individual nanostructures lack in-plane symmetry, their overall arrangements are random. This lack of in-plane symmetry does not significantly affect the operation of the nanostructure-based devices. Unlike thin films, which require precise merging for functionality, nanostructure arrays operate as an ensemble, with numerous individual nanostructures collectively

contributing to the overall device performance. Choi et al. deposited a 150 nm-thick Ti preorienting layer on a glass substrate.^[30] Titanium has a hexagonal crystal structure with a lattice mismatch of 7.4% with GaN. As a result, polycrystalline GaN grown on a Ti preorienting layer using MOCVD showed superior *c*-plane orientation compared to GaN grown directly on bare glass. Subsequently, SiO₂ hole patterns were created via lithography and nanopillars were grown using the SAG method via MOCVD. Figure 4a illustrates the *p-i-n* nanopillar structure, where the Ti preorienting

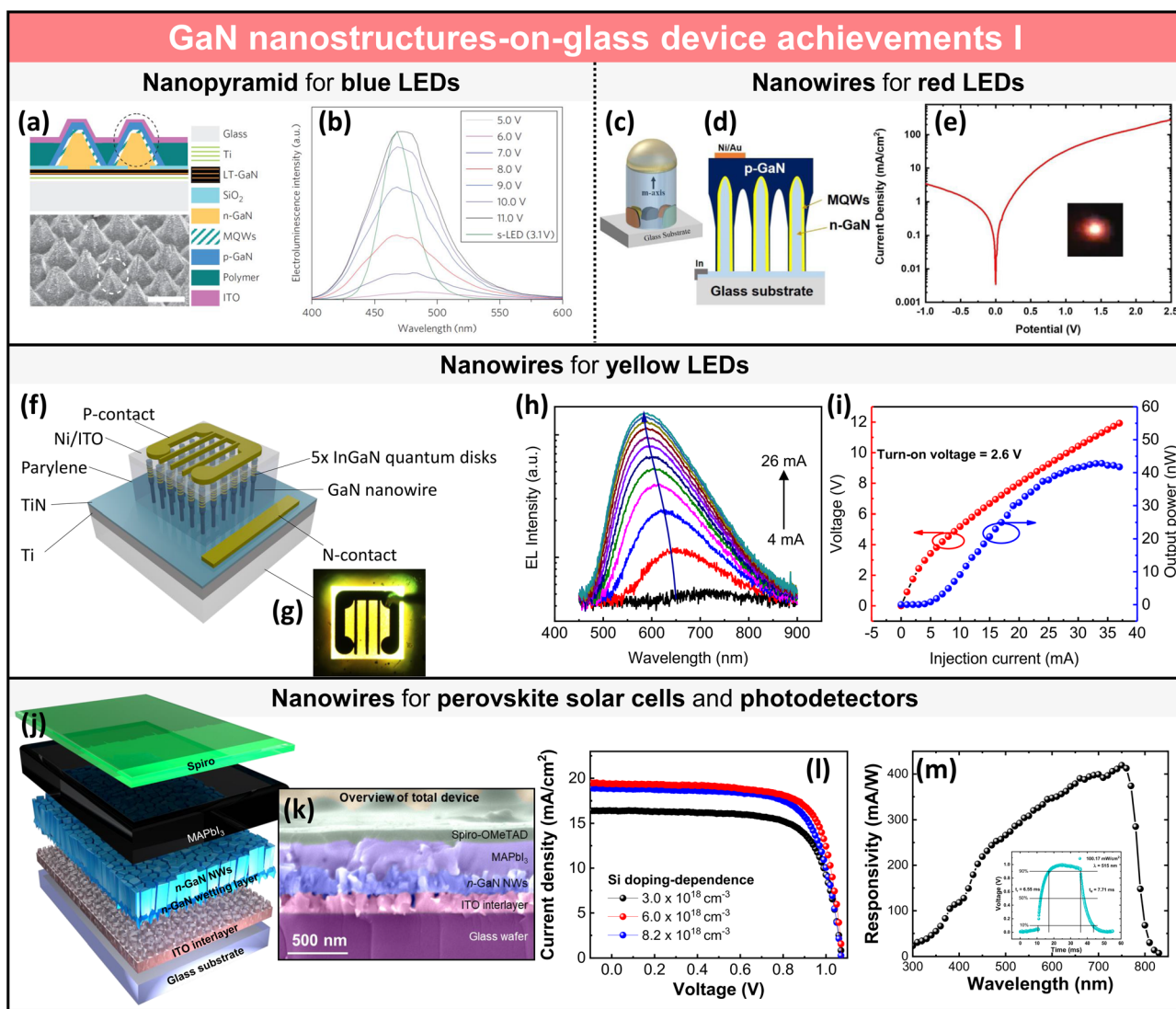


Figure 4. a) Schematic representation and SEM tilted view of MOCVD-grown GaN nanopillars using the SAG method on a Ti-coated glass substrate. b) EL spectra of the nanopillar LED structure under varying voltages. Reproduced with permission.^[30] Copyright 2011, Nature Portfolio. c) Schematic representation of the evolution of MOCVD-grown GaN nanowires on a glass substrate, controlled by a metal alloy catalyst. d) Schematic illustration of a complete nanowire-based red LED structure. e) I–V characteristic of the nanowire-based red LED. The inset shows an optical photograph of the PL emission from nanowire-based red LED. Reproduced with permission.^[29] Copyright 2020, Elsevier. f) Schematic representation of a nanowire-based LED structure grown by PA-MBE on a Ti-coated glass substrate. g) Optical photograph of the nanowire-based yellow LED. h) EL spectra of the nanowire-based yellow LED under varying injection currents. i) L–I–V characteristics of the nanowire-based yellow LED. Reproduced with permission.^[93] Copyright 2019, Springer. j) Schematic representation of an MAPbI₃ PSC device with n-type GaN nanowires-on-glass as an ETL. k) False-color cross-sectional SEM image of the device. l) Photovoltaic parameters of three different Si doping concentrations in GaN nanowires-on-glass ETL under AM 1.5 G with 1 sun illumination. m) Spectral responsivity and rise and fall times calculated at a light intensity of 100.17 mW cm^{−2} (20 Hz). Reproduced with permission.^[94] Copyright 2024, Wiley-VCH.

layer provides *c*-plane orientation and serves as a reflector. LED fabrication performed by a planarization process using a polymer. Figure 4b shows the electroluminescence (EL) spectrum of the device. This is the first demonstration of LED operation on an amorphous glass substrate with a blue LED emitting at a central wavelength of 448–478 nm.

In addition to the high-cost SAG method, the low-cost VLS growth method has been employed to fabricate nanowire arrays on glass substrates. Kuykendall et al. reported that the liquid metal-nanowire interfacial energy determined the growth direction when Au catalysts were used, promoting the growth of *m*-plane GaN nanowires along the (1-100) direction.^[92] Similarly, Johar et al. demonstrated the growth of *m*-plane GaN nanowires via MOCVD using Au/In/Ga metal alloy catalysts.^[29] Subsequently, a uniform InGa_{0.5}N/GaN core-shell structure with a triangular cross-section was grown along the semipolar (11–22) plane. Figure 4c illustrates the growth process of the nanowires, and Figure 4d shows a schematic of the LED device structure. The p-type GaN regions coalesced, eliminating the need for additional planarization. Figure 4e also shows the I–V curve and an optical photograph of the PL emission from the nanowire-based red LED (inset). This device achieved a high quantum efficiency of 76.1%, with suppressed quantum-confined Stark effects.

When the VLS method was used, a GaN wetting layer formed at the interface between the GaN nanowires and glass substrate; however, obtaining the EL spectra proved challenging. Prabaswara et al. investigated GaN nanowires grown via PAMBE on a 20-nm-thick Ti preorienting layer deposited on a glass substrate.^[93] The Ti layer was exposed to nitrogen plasma to form a TiN layer, which improved the transmittance approximately twofold, from 22% to 42%, at a visible wavelength of 550 nm. The TiN/Ti layer on the glass served as a translucent conductive layer and maintained similar transmittance even after the growth of the *p-i-n* nanowire-based yellow LED structure. Figure 4f shows a schematic of the LED structure, and the corresponding optical photograph (Figure 4g) shows the EL spectra emitting yellow light. The nanowire-based yellow LED operated stably and exhibiting EL spectra in the red-amber-yellow range. A blue shift in the center wavelength from 650 to 590 nm was observed with increasing injection current, as shown in Figure 4h. The luminance–current–voltage (L–I–V) characteristics in Figure 4i reveal a turn-on voltage of 2.6 V and a turn-on resistance of 300 Ω.

GaN grown on a TCL is a strong candidate for optoelectronic device applications via heterogeneous integration with other material platforms. One example is the combination of PSCs with n-type GaN nanowires as the electron transport layer (ETL). GaN nanowires were grown on ITO coalescent columnar grains using PAMBE with a two-step growth method to form a GaN wetting layer at the GaN nanowires/ITO interface. After spin-coating the light-absorbing layer MAPbI₃ onto n-type GaN nanowires, spiro-OMeTAD was applied as a hole transport layer to complete the PSC structure. Figure 4j shows a schematic representation of the PSC structure, and the cross-sectional SEM image in Figure 4k shows well-separated interfaces.^[94] Prior to device operation, optical simulations confirmed that the GaN wetting layer and n-type GaN nanowire ETL effectively absorbed UV light while allowing visible light to pass through the MAPbI₃ layer without significant absorption. Figure 4l shows that the Si

doping level of the n-type GaN nanowire ETL was optimized using Mott-Schottky measurements, achieving a power conversion efficiency of 15.67% at an electron concentration of $6 \times 10^{18} \text{ cm}^{-3}$. The peak EQE was $\approx 71.9\%$, which corresponded to a spectral responsivity of 420 mA W^{-1} at 750 nm for the 300–800 nm range (Figure 4m). The inset shows the response characteristics of the PSC device when modulated by a 520 nm laser with an intensity of $100.17 \text{ mW cm}^{-2}$, indicating rise and fall times of 6.55 ms and 7.71 ms, respectively, demonstrating its functionality as a PD. Unlike GaN grown on highly insulating sapphire substrates or nontransparent Si substrates, GaN grown on TCL enables seamless integration with other materials. This approach introduces a new concept expanding the applications of optoelectronic devices.

4.3. Growth of Single-Crystalline GaN Thin Films

Unlike nanostructures, growing a single-crystalline GaN thin film on a glass substrate requires inheriting the in-plane symmetry from the preorienting layer. This is a critical factor in achieving single-crystalline GaN properties after nucleation and merging. As demonstrated in the case of GaN grown on MXene nanoflakes, the use of 2D materials as preorienting layers presents an optimal approach for this goal. In particular, PVD operates at significantly lower growth temperatures than conventional MOCVD, making it well-suited for utilizing substrates with low softening temperatures, such as glass, in GaN-based devices. Shon et al. used PSD to employ multilayer graphene (MLG) as a preorienting layer on a Si(100) substrate coated with a 100-nm-thick amorphous SiO₂ layer.^[95] The thick Si(100) substrate effectively absorbed and efficiently transferred heat to GaN grown on the amorphous SiO₂ layer. Figure 5a,b presents the EBSD measurements of the GaN thin films grown on the MLG preorienting layer. Notably, the absence of an AlN buffer layer resulted in the coexistence of the zincblende and wurtzite phases, with the zincblende phase constituting $\approx 45\%$. In contrast, the inclusion of the AlN buffer led to the exclusive presence of the wurtzite phase. Figure 5c shows the XRD $2\theta/\omega$ scan results, indicating peaks corresponding to the (002) and (004) planes of wurtzite GaN and the Si(400) plane. Figure 5d,e shows the EBSD results, where the (002) point exhibits distinct *c*-plane orientation, and the spots measured at (102) demonstrate perfect sixfold rotational symmetry.

Xu et al. made a similar attempt using MoN as a preorienting layer on a glass substrate.^[96] The lattice mismatch between hexagonal (001) σ -MoN and hexagonal (001) GaN is only 11.1%, which is smaller than the lattice mismatch between GaN and sapphire or Si(111). Figure 5f schematically represents PAMBE-grown GaN thin films. XRD 2θ -scan results (Figure 5g) and (102) ϕ -scan measurements (Figure 5h) confirmed the wurtzite structure and perfect sixfold rotational symmetry. WS₂ is another promising candidate for a preorienting layer. Yin et al. demonstrated that WS₂ is advantageous for GaN epitaxy owing to its polarity matching.^[97] Figure 5i shows a schematic of the GaN growth process. XRD analysis confirmed the wurtzite structure of the GaN film, with a (002) rocking curve FWHM of 1.6° . Figure 5j presents the XRD (103) ϕ -scan results, showing sixfold in-plane symmetry. These 2D materials, including graphene,

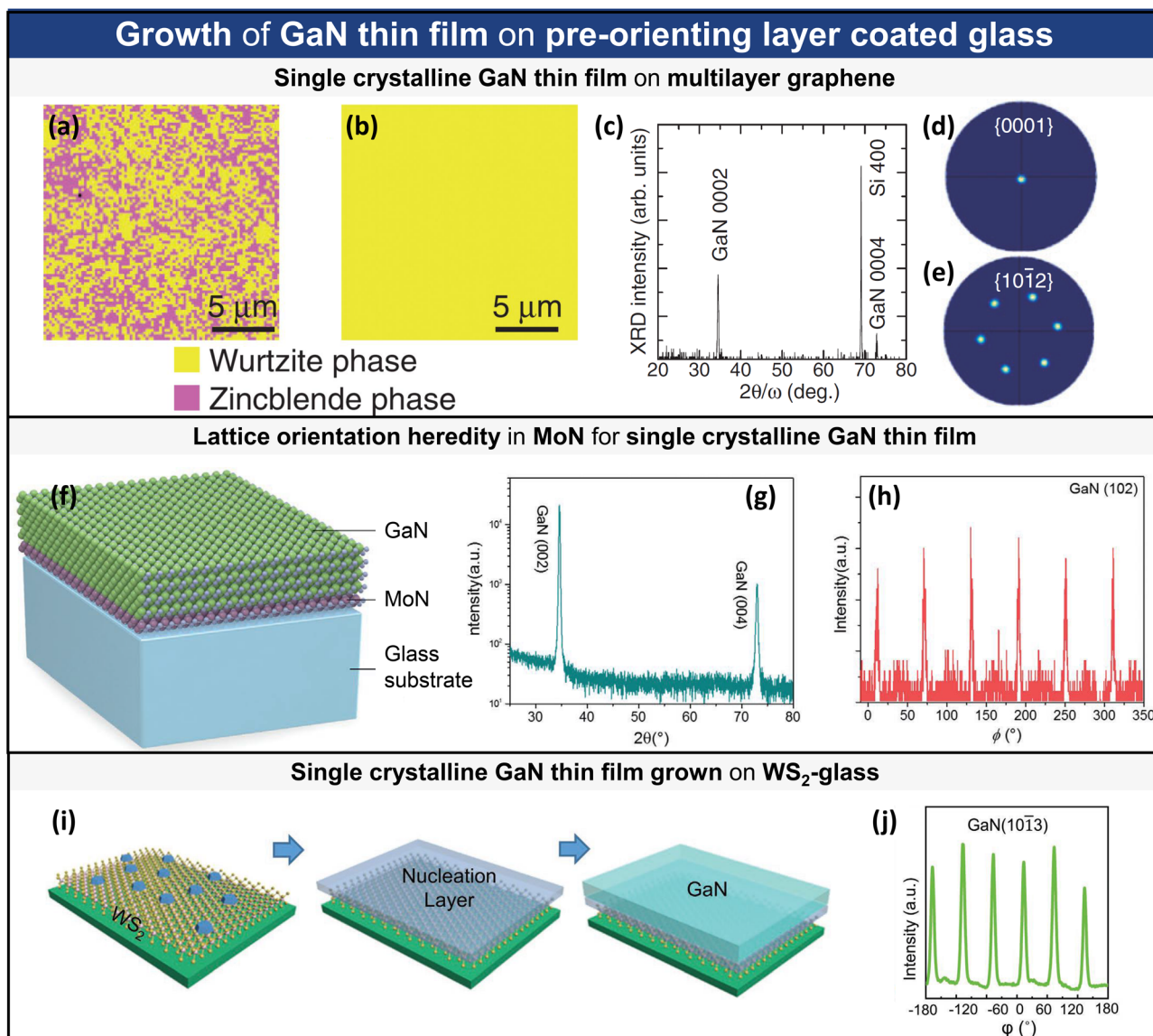


Figure 5. EBSD scan results of GaN thin film grown on multilayer graphene a) without and b) with AlN interlayers on an amorphous-SiO₂/Si substrate. c) XRD $2\theta/\omega$ scan measurement results and EBSD results for d) {002} and e) {102} planes of the GaN thin film on an amorphous-SiO₂/Si substrate. Reproduced with permission.^[95] Copyright 2014, IOP Publishing Ltd. f) Schematic representation of a GaN thin film on a MoN/glass substrate. XRD g) 2θ -scan and h) (102) ϕ -scan measurement results of the GaN thin film on a MoN/glass substrate. Reproduced with permission.^[96] Copyright 2021, Wiley-VCH. i) Schematic representation of the evolution of GaN thin film on a WS₂/glass substrate and j) XRD (103) ϕ -scan measurement of the sample. Reproduced with permission.^[97] Copyright 2022, Wiley-VCH.

MoN, and WS₂, have demonstrated exceptional orientation guidance as preorienting layers for growing single-crystalline GaN thin films on glass substrates, paving the way for advanced optoelectronic applications.

4.4. Optoelectronic Device Applications of GaN Thin Films on Glass

Using a 2D material as a preorienting layer, the in-plane rotational symmetry can be transferred to the GaN grown on top. This process is generally attributed to the van der Waals epitaxy mechanism, which enables high-quality material growth despite

the lattice mismatch between 2D materials and III-nitride semiconductors. The resulting single-crystalline GaN thin film exhibits excellent crystalline quality and conductivity, making it suitable for device operation. **Figure 6a** shows the GaN thin film growth procedure on a graphene-coated amorphous SiO₂/Si(100) substrate. Notably, the graphene layer used in this study was synthesized via CVD rather than by transfer. The graphene synthesized on the SiO₂/Si(100) substrate at 1050 °C for 5 h in a furnace achieved large-scale uniform coverage with a thickness of ≈ 1 –5 layers. Subsequently, the AlN buffer layer was grown at 1200 °C. The low energy barrier for the slip and rotation of AlN on graphene allows the AlN nuclei to align easily at high

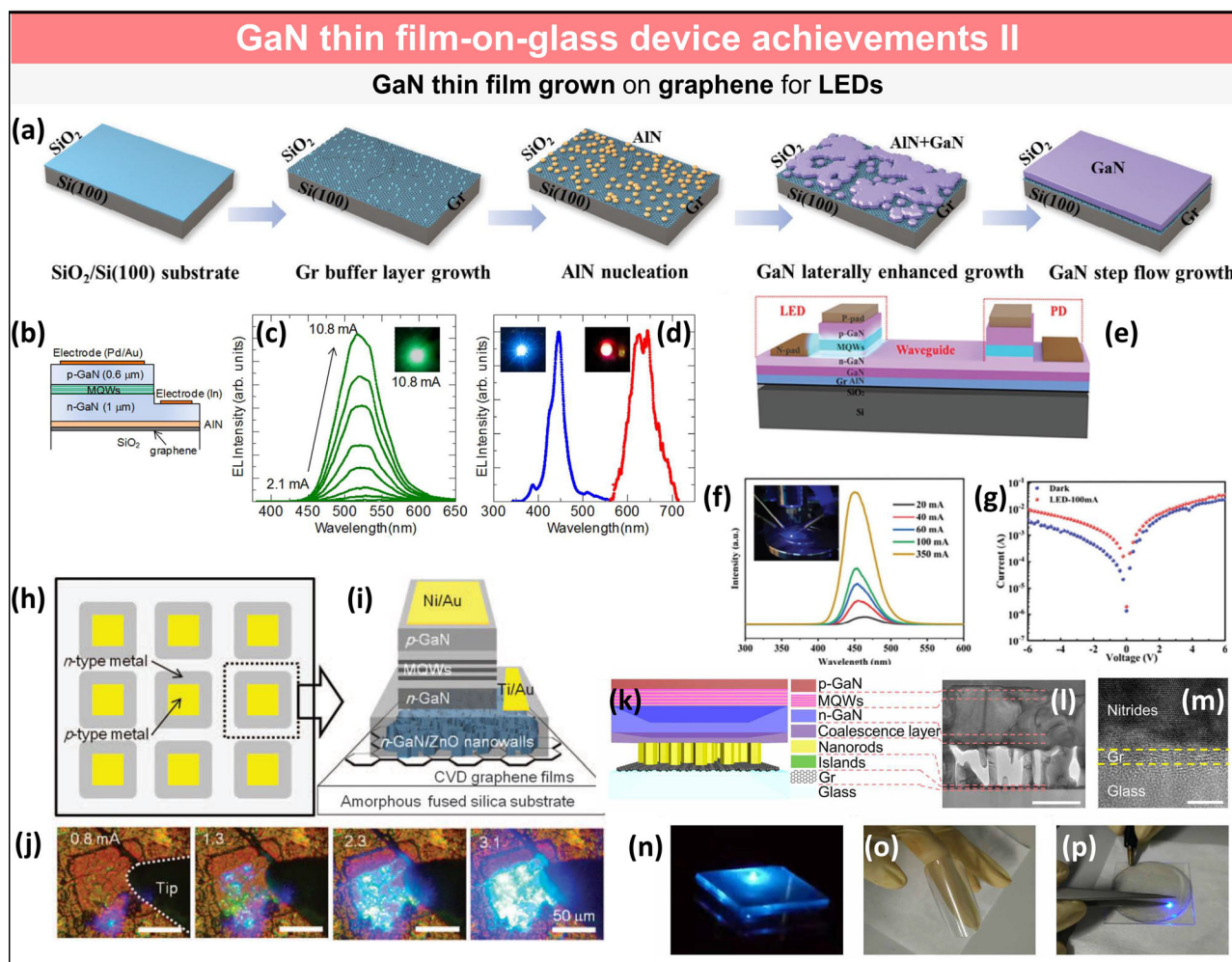


Figure 6. a) Schematic representation of the evolution of a GaN thin film on graphene on an amorphous SiO_2/Si substrate. Reproduced with permission.^[111] Copyright 2024, Wiley. b) Schematic representation of a PSD-grown GaN thin film LED structure on a multilayer graphene/glass substrate. c) EL spectra for the green LED under varying injection currents and photographs and EL spectra for d) blue and red LEDs. Reproduced with permission.^[57] Copyright 2014, Nature Portfolio. e) Schematic representation of on-chip integrated devices comprising GaN thin film LED and PD on graphene on an amorphous SiO_2/Si substrate. f) EL spectra of the blue LED under varying injection currents. g) I–V curves of the PD corresponding to illumination from the LED (operated at 0 and 100 mA). Reproduced with permission.^[111] Copyright 2024, Wiley. h) Schematic representation of an array of GaN thin film LED pixels and i) a single blue LED on an n-type GaN/ZnO/graphene/glass substrate. j) Optical photograph of EL emission under varying injection currents. Reproduced with permission.^[98] Copyright 2012, Nature Portfolio. k) Schematic representation of a GaN blue LED structure on a graphene/glass substrate and l) cross-sectional TEM image of the structure. m) High-resolution TEM image at the GaN/graphene interface. Optical photographs of n) a blue LED at room temperature showing blue luminescence, o) a flexible blue LED exfoliated from the glass substrate, and p) blue luminescence from the flexible blue LED. Reproduced with permission.^[53] Copyright 2021, American Association for the Advancement of Science.

temperatures, forming larger islands that merge to create a highly crystalline GaN thin film with sufficient conductivity for device operation.

Figure 6b shows the first thin-film LED grown on an MLG-coated glass substrate using this method. Shon et al. demonstrated a green LED with an adjustable intensity based on injection current, as shown in the EL spectra in Figure 6c.^[57] The LED was grown using a PSD, and by varying the indium composition in the active layer, they also obtained EL spectra for blue and red LEDs, indicating the feasibility of full-color RGB LEDs on amorphous glass substrate (Figure 6d). Figure 6e shows a schematic of a single-chip device integrating a blue LED and a PD on a $\text{SiO}_2/\text{Si}(100)$ substrate.

The InGaN/GaN multiquantum well (MQW) used as the active layer for the blue LED also served as the photodetection layer for the PD. Figure 6f shows EL spectra with a blue shift from 462.1 nm to 453.2 nm, and the inset displays an optical photograph of the LED emission. For PD operation, the device exhibited a dark current of 2.49×10^{-7} A at zero bias, while under blue LED illumination, the photocurrent reached 3.24×10^{-6} A (Figure 6g). The responsivity was measured at 2.01×10^5 A W⁻¹, and the response time (rise and fall times of 248 and 129 μ s, respectively) demonstrated significant potential for rapid response.

In addition to thin-film devices using AlN buffers on 2D material preorienting layers, alternative approaches involving hybrid

heterostructures have also been explored. Chung et al. used MOCVD-grown ZnO nanowalls as a buffer layer on graphene with a height of 200–400 nm and density of 10^{10} cm^{-2} .^[98] The subsequent GaN epitaxial layer exhibited a high quality. Figure 6h,i shows schematic representations of the array-type pixel LEDs, which display a strong EL even under room illumination (Figure 6j). Ren et al. further advanced this research by introducing GaN epitaxy onto graphene-coated glass substrates using nanorods.^[53] The nanorod formation maintained only three major in-plane orientations, enabling the coalesced GaN to achieve high crystalline quality. Figure 6k shows a schematic of the LED structure grown on this surface, and the cross-sectional TEM image in Figure 6l shows a fully coalesced n-type GaN thin film. The high-resolution TEM image in Figure 6m confirms that the graphene preorienting layer remains stable at the GaN/graphene interface. The fabricated blue LED exhibited blue luminescence, as shown in Figure 6n. Epitaxial growth on 2D material preorienting layers follows the van der Waals epitaxy mechanism, which enables easy exfoliation of the epitaxial structure using methods such as thermal release tape. Figure 6o shows an optical photograph image of the epitaxial structure of the exfoliated blue LED. This structure demonstrates strong EL characteristics at $\approx 477 \text{ nm}$, as evidenced by the emission device shown in Figure 6p. Hybrid heterostructures incorporating 2D preorienting layers provide a functional material system for the development of innovative optoelectronic devices on amorphous glass substrates. Moreover, their stable operation in optoelectronic devices has introduced new possibilities for their applications on amorphous substrates.

5. Discussion and Conclusions

5.1. Key Summary and Insights

The exploration of GaN growth on amorphous glass substrates represents a transformative step toward the realization of cost-effective and scalable optoelectronic devices. Advances in epitaxial methods, including MOCVD, PA-MBE, and PSD, have enabled researchers to make significant progress in the development of high-quality GaN thin films and nanostructures on glass, addressing challenges such as the lack of global epitaxy. The introduction of preorienting layers, such as ITO and Ti metal layers, and 2D materials, such as graphene, MXene, WS_2 , and MoN, has further facilitated improved crystallinity, in-plane rotational symmetry, and enhanced device functionality. These innovations have led to the successful fabrication of LEDs, PDs, and hybrid heterostructures, with applications ranging from full-color displays to integrated systems. Future research will likely emphasize refining heterostructure designs, improving material compatibility, and achieving precise control over crystal orientation and defect density. Such advancements are expected to pave the way for high-performance, energy-efficient devices, firmly positioning GaN-on-glass technology as a cornerstone for next-generation optoelectronics and photonics.

5.2. Potential Applications

One of the most promising applications of GaN-on-glass technology is in monolithic micro-LED displays. Direct epitaxial growth

of GaN LED pixels onto a glass substrate (similar to depositing organic films on thin-film transistor glass for organic LED (OLED)) allows manufacturing of an entire display in a single process, thereby eliminating the mass transfer of tiny LED chips.^[57] This approach significantly reduces the pick-and-place step, which has long been a bottleneck for micro-LED prototypes.^[99] Compared to both OLED and liquid crystal displays (LCD), monolithic GaN micro-LED displays offer multiple advantages. Unlike OLEDs, the inorganic nature of GaN LED enables them to withstand high brightness without degradation or burn-in. Indeed, micro LEDs have demonstrated exceptionally high luminance, far surpassing the $\approx 500\text{--}1000 \text{ cd m}^{-2}$ typical of OLED.^[100,101] Meanwhile, LCDs inevitably suffer from limited contrast owing to the constantly operating backlight; however, but micro-LED can switch off individual pixels for essentially infinite contrast. Furthermore, the inherent durability and efficiency of inorganic LEDs allow them to maintain their brightness and long operational lifetimes even under continuous high-brightness conditions.^[102,103] Structurally, micro-LED displays are much simpler than LCDs, enabling lower power consumption and thinner form factors. One might say that they combine the thin, self-emissive nature of OLED with the high efficiency and robust lifespan of inorganic LEDs.

In addition, glass substrates can be made transparent or extremely thin, allowing for transparent or flexible displays. For example, transparent micro-LEDs can be integrated into heads-up displays (HUDs) or augmented reality (AR) glasses. iBeam Materials is developing a GaN-on-X process that grows GaN micro-LEDs on metal foils or other substrates, yielding devices that are ultrathin and flexible while maintaining high performance.^[104–106] Researchers have also explored the direct integration of drive circuitry on the same substrate, to facilitate an all-in-one drive and emission matrix.^[107–109] Further possibilities include bonding wafer-scale micro-LED arrays to standard display backplanes or, ultimately, epitaxially growing both LEDs and drive electronics on the glass itself to eliminate additional process steps. Ultimately, the prospect of directly growing large-area, ultrabright, long-lifetime micro-LED arrays on glass could redefine the display paradigm.

5.3. Challenges and Future Outlook

Despite these remarkable advances, GaN-on-glass still faces several technical challenges in commercialization. The first is the crystallinity and defect density. GaN grown on amorphous glass frequently exhibits a greater lattice mosaicity and higher dislocation density than GaN grown on single-crystal wafers. Early attempts mostly produced random polycrystalline films, although the use of 2D material preorienting layers has helped to significantly reduce the number of in-plane orientations. Careful control of nucleation and domain coalescence remains essential for scaling uniformly over large area.

The second challenge is thermal management. Most display-grade glass deforms around at $\approx 600^\circ\text{C}$, and plastic glass substrates tolerate even lower temperatures, whereas high-quality GaN typically requires $\approx 1000^\circ\text{C}$. Low-temperature MOCVD, low-temperature MBE, and plasma-assisted growth methods have been investigated to bridge this gap. For example, BluGlass reported that

its remote plasma CVD (RPCVD) process can achieve high-quality GaN at temperatures much lower than those required for conventional MOCVD.^[110]

The third issue concerns polarity control and interface engineering. GaN grows differently depending on whether the Ga- or N-polar face is exposed, and mixed-polarity domains can be easily formed on an amorphous substrate.^[57,81] Avoiding this may require the establishment of a uniform polarity at the nucleation stage or the inserting of 2D layers to induce a selective orientation. If the underlying substrate is crystalline, then remote epitaxy effects, that is, partial electrostatic interactions penetrating the 2D layer, can also be leveraged to influence GaN ordering. In the future, wafer-scale single-crystal graphene or *h*-BN can be transferred or formed onto glass, providing a template for GaN epitaxy.

Industries and academia are already pursuing innovative solutions to these issues. As mentioned previously, BluGlass addresses thermal issues with RPCVD, whereas iBeam Materials' GaN-on-X uses IBAD to establish oriented buffer layers on virtually any substrate for growing GaN LEDs. Such roll-to-roll manufacturing enables the fabrication of massive low-cost GaN-on-glass displays. Researchers have continued to explore 2D material-assisted growth, remote epitaxy, nanoscale texturing, and advanced in situ monitoring to optimize nucleation and coalescence.

In summary, while GaN-on-glass has progressed rapidly in recent years, key tasks have focused on low-temperature epitaxy, van der Waals epitaxy, and polarity/interface control before achieving full commercial adoption. Nevertheless, the success of glass-based LED demonstrations of quasi-single-crystalline films and flexible devices indicates the superiority of these barriers. The coming years, in which research innovation will transition into commercial products, will be pivotal and the future of GaN-on-glass will appear bright.

Acknowledgements

The authors would like to acknowledge the support from the National Research Foundation of Korea (NRF) grant funded by the Korean government (MSIT) (RS-2023-00244550 and NRF-2022R1F1A1064130).

Conflict of Interest

The authors declare no conflict of interest.

Keywords

GaN, GaN-on-glass, III-nitrides, nanowires

Received: January 28, 2025

Revised: May 21, 2025

Published online:

- [1] L. F. Jiang, W. Z. Shen, Q. X. Guo, *J. Appl. Phys.* **2009**, 106, 1.
- [2] P. Schley, R. Goldhahn, A. T. Winzer, G. Gobsch, V. Cimalla, O. Ambacher, H. Lu, W. J. Schaff, M. Kurouchi, Y. Nanishi, M. Rakel, C. Cobet, N. Esser, *Phys. Rev. B* **2007**, 75, 205204.

- [3] H. S. Jung, Y. J. Hong, Y. Li, J. Cho, Y.-J. Kim, G.-C. Yi, *ACS Nano* **2008**, 2, 637.
- [4] S. Zhao, O. Salehzadeh, S. Alagha, K. L. Kavanagh, S. P. Watkins, Z. Mi, *Appl. Phys. Lett.* **2013**, 102, 7.
- [5] F. Scholz, *Semicond. Sci. Technol.* **2012**, 27, 024002.
- [6] C. Zhao, N. Alfaraj, R. C. Subedi, J. W. Liang, A. A. Alatawi, A. A. Alhamoud, M. Ebaid, M. S. Alias, T. K. Ng, B. S. Ooi, *Prog. Quantum Electron.* **2018**, 61, 1.
- [7] J. H. Choi, J. Kim, H. Yoo, J. Liu, S. Kim, C.-W. Baik, C.-R. Cho, J. G. Kang, M. Kim, P. V. Braun, S. Hwang, T.-S. Jung, *Adv. Opt. Mater.* **2016**, 4, 505.
- [8] J. T. Kohli, M. Hubert, R. E. Youngman, D. L. Morse, *International Journal of Applied Glass Science* **2022**, 13, 292.
- [9] M. Montazerian, S. P. Singh, E. D. Zanolto, *Am. Ceram. Soc. Bull.* **2015**, 94, 30.
- [10] E. D. Zanolto, *Am. Ceram. Soc. Bull.* **2010**, 89, 19.
- [11] A. L. Mitchell, D. E. Perea, M. G. Wirth, J. V. Ryan, R. E. Youngman, A. Rezikyan, A. J. Fahey, D. K. Schreiber, *Scr. Mater.* **2021**, 203, 114110.
- [12] R. Kitamura, L. Pilon, M. Jonasz, *Appl. Opt.* **2007**, 46, 8118.
- [13] J. E. Shelby, *Royal Society of Chemistry*, **2020**.
- [14] P. C. Tsai, R. W. Chuang, Y. K. Su, *J. Lightwave Technol.* **2007**, 25, 591.
- [15] A. J. Trindade, B. Guilhabert, E. Y. Xie, R. Ferreira, J. J. D. McKendry, D. Zhu, N. Laurand, E. Gu, D. J. Wallis, I. M. Watson, C. J. Humphreys, M. D. Dawson, *Opt. Express* **2015**, 23, 9329.
- [16] B. Lu, T. Palacios, *IEEE Electron Device Lett.* **2010**, 31, 951.
- [17] M. Haziq, S. Falina, A. A. Manaf, H. Kawarada, M. Syamsul, *Micromachines* **2022**, 13, 2133.
- [18] B. Benbakhti, A. Soltani, K. Kalna, M. Rousseau, J.-C. De Jaeger, *IEEE Trans. Electron Devices* **2009**, 56, 2178.
- [19] M. Nazari, B. L. Hancock, E. L. Piner, M. W. Holtz, *IEEE Trans. Electron Devices* **2015**, 62, 1467.
- [20] A. Wang, L. Zeng, W. Wang, *AIP Adv.* **2017**, 7, 9.
- [21] J.-B. Park, J.-S. Ha, T. Jeong, *ECS Meeting Abstracts*, MA2020-02 **2020**, 42, 2732.
- [22] P. Wei Chih, W. YewChung Sermon, *IEEE Photonics Technol. Lett.* **2006**, 18, 613.
- [23] Y. Yu, T. Wang, X. Chen, L. Zhang, Y. Wang, Y. Niu, J. Yu, H. Ma, X. Li, F. Liu, G. Deng, Z. Shi, B. Zhang, X. Wang, Y. Zhang, *Light: Sci. Appl.* **2021**, 10, 117.
- [24] E. Richter, C. Hennig, M. Weyers, F. Habel, J.-D. Tsay, W.-Y. Liu, P. Brückner, F. Scholz, Y. Makarov, A. Segal, J. Kaeppler, *J. Cryst. Growth* **2005**, 277, 6.
- [25] P. Rouf, N. J. O'Brien, S. C. Buttera, I. Martinovic, B. Bakht, E. Martinsson, J. Palisaitis, C.-W. Hsu, H. Pedersen, *J. Mater. Chem. C* **2020**, 8, 8457.
- [26] C. M. Furqan, J. Y. L. Ho, H. S. Kwok, *Surf. Interfaces* **2021**, 26, 101364.
- [27] B. Heying, R. Averbeck, L. F. Chen, E. Haus, H. Riecher, J. S. Speck, *J. Appl. Phys.* **2000**, 88, 1855.
- [28] R. D. Vispute, V. Talyansky, R. P. Sharma, S. Choopun, M. Downes, T. Venkatesan, K. A. Jones, A. A. Iliadis, M. A. Khan, J. W. Yang, *Appl. Phys. Lett.* **1997**, 71, 102.
- [29] M. A. Johar, H.-G. Song, A. Waseem, M. A. Hassan, I. V. Bagal, Y.-H. Cho, S.-W. Ryu, *Appl. Mater. Today* **2020**, 19, 100541.
- [30] J. H. Choi, A. Zoukarneev, S. I. Kim, C. W. Baik, M. H. Yang, S. S. Park, H. Suh, U. J. Kim, H. B. Son, J. S. Lee, M. Kim, J. M. Kim, K. Kim, *Nat. Photonics* **2011**, 5, 763.
- [31] S. Kim, Y. Lee, D. Moon, *J. Korean Phys. Soc.* **1998**, 33, L1–L1.
- [32] H. Yu, L. Chen, R. Zhang, X. Q. Xiu, Z. L. Xie, Y. D. Ye, S. L. Gu, B. Shen, Y. Shi, Y. D. Zheng, *In Materials Science Forum* **2005**, vol. 475, Trans Tech Publications, pp. 3783–3786.
- [33] N. Grandjean, J. Massies, Y. Martinez, P. Vennéguès, M. Leroux, M. Lügt, *J. Cryst. Growth* **1997**, 178, 220.

- [34] Y. Sato, A. Kurosaki, S. Sato, *J. Cryst. Growth* **1998**, 189–190, 42.
- [35] C. W. Zou, H. J. Wang, M. L. Yin, M. Li, C. S. Liu, L. P. Guo, D. J. Fu, T. W. Kang, *J. Cryst. Growth* **2009**, 311, 223.
- [36] A. L. Mulyo, Y. Konno, J. S. Nilsen, A. T. J. van Helvoort, B.-O. Fimland, H. Weman, K. Kishino, *J. Cryst. Growth* **2017**, 480, 67.
- [37] A. Kikuchi, K. Yamano, M. Tada, K. Kishino, *Phys. Status Solidi B* **2004**, 241, 2754.
- [38] W.-S. Liu, Y.-L. Chang, H.-Y. Chen, *Coatings* **2019**, 9, 419.
- [39] F. Adibi, I. Petrov, J. E. Greene, L. Hultman, J.-E. Sundgren, *J. Appl. Phys.* **1993**, 73, 8580.
- [40] T. Araki, H. Kagatsume, T. Noguchi, T. Maruyama, Y. Nanishi, *Phys. Status Solidi C* **2003**, 1, 200.
- [41] H. X. Wang, T. Wang, M. Lachab, Y. Ishikawa, M. S. Hao, K. Oyama, K. Nishino, S. Sakai, K. Tominaga, *J. Cryst. Growth* **1999**, 206, 241.
- [42] K. Chung, H. Oh, J. Jo, K. Lee, M. Kim, G.-C. Yi, *NPG Asia Mater.* **2017**, 9, e410.
- [43] J. Yu, J. Wang, W. Yu, C. Wu, B. Lu, J. Deng, Z. Zhang, X. Li, Z. Hao, L. Wang, Y. Han, Y. Luo, C. Sun, B. Xiong, H. Li, *Thin Solid Films* **2018**, 662, 174.
- [44] M. Yoshizawa, A. Kikuchi, M. Mori, N. Fujita, K. Kishino, *Jpn. J. Appl. Phys.* **1997**, 36, L459.
- [45] V. Consonni, M. Hanke, M. Knelangen, L. Geelhaar, A. Trampert, H. Riechert, *Phys. Rev. B* **2011**, 83, 035310.
- [46] Ž. Gačević, A. Bengoechea-Encabo, S. Albert, J. Appl. Phys. **2015**, 117, 3.
- [47] H.-W. Lin, Y.-J. Lu, H.-Y. Chen, H.-M. Lee, S. Gwo, *Appl. Phys. Lett.* **2010**, 97, 7.
- [48] H. Sekiguchi, K. Kato, J. Tanaka, A. Kikuchi, K. Kishino, *Phys. Status Solidi A* **2008**, 205, 1067.
- [49] K. P. Korona, A. Reszka, M. Sobanska, P. S. Perkowska, A. Wyszomolek, K. Klosek, Z. R. Zytewicz, *J. Lumin.* **2014**, 155, 293.
- [50] Z. Bougrioua, P. Gibart, E. Calleja, U. Jahn, A. Trampert, J. Ristic, M. Utrera, G. Nataf, *J. Cryst. Growth* **2007**, 309, 113.
- [51] B. H. Le, S. Zhao, X. Liu, S. Y. Woo, G. A. Botton, Z. Mi, *Adv. Mater.* **2016**, 28, 8446.
- [52] R. T. ElAfandy, M. Ebaid, J.-W. Min, C. Zhao, T. K. Ng, B. S. Ooi, *Opt. Express* **2018**, 26, A640.
- [53] F. Ren, B. Liu, Z. Chen, Y. Yin, J. Sun, S. Zhang, B. Jiang, B. Liu, Z. Liu, J. Wang, M. Liang, *Sci. Adv.* **2021**, 7, 31, eabf5011.
- [54] Y. Kim, S. S. Cruz, K. Lee, B. O. Alawode, C. Choi, Y. Song, J. M. Johnson, C. Heidelberger, W. Kong, S. Choi, K. Qiao, I. Almansouri, E. A. Fitzgerald, J. Kong, A. M. Kolpak, J. Hwang, J. Kim, *Nature* **2017**, 544, 340.
- [55] W. Kong, H. Li, K. Qiao, Y. Kim, K. Lee, Y. Nie, D. Lee, T. Osadchy, R. J. Molnar, D. K. Gaskill, R. L. Myers-Ward, K. M. Daniels, Y. Zhang, S. Sundram, Y. Yu, S.-h. Bae, S. Rajan, Y. Shao-Horn, K. Cho, A. Ougazzaden, J. C. Grossman, J. Kim, *Nat. Mater.* **2018**, 17, 999.
- [56] F. Liu, T. Wang, X. Gao, H. Yang, Z. Zhang, Y. Guo, Y. Yuan, Z. Huang, J. Tang, B. Sheng, Z. Chen, K. Liu, B. Shen, X.-Z. Li, H. Peng, X. Wang, *Sci. Adv.* **2023**, 9, 31.
- [57] J. W. Shon, J. Ohta, K. Ueno, A. Kobayashi, H. Fujioka, *Sci. Rep.* **2014**, 4, 5325.
- [58] S.-M. Lee, J.-H. Kim, J.-H. Ahn, *Mater. Today* **2015**, 18, 336.
- [59] J.-H. Park, X. Yang, J.-Y. Lee, M.-D. Park, S.-Y. Bae, M. Pristovsek, H. Amano, D.-S. Lee, *Chem. Sci.* **2021**, 12, 7713.
- [60] H.-M. Kwak, J.-S. Lee, B.-I. Park, J. Baik, J. Kim, W.-L. Jeong, K.-P. Kim, S.-H. Mun, H. Kim, J. Kim, D.-S. Lee, *ACS Nano* **2023**, 17, 11739.
- [61] L. van Deurzen, E. Kim, N. Pieczulewski, Z. Zhang, A. Feduniewicz-Zmuda, M. Chlipala, M. Siekacz, D. Muller, H. G. Xing, D. Jena, H. Turski, *Nature* **2024**, 634, 334.
- [62] R. Collazo, S. Mita, A. Aleksov, R. Schlessner, Z. Sitar, *J. Cryst. Growth* **2006**, 287, 586.
- [63] Y. Xia, J. Brault, P. Vennéguès, M. Nemoz, M. Teisseire, M. Leroux, J.-M. Chauveau, *J. Cryst. Growth* **2014**, 388, 35.
- [64] A.-H. Park, T.-H. Seo, *Materials* **2023**, 16, 7216.
- [65] F. Liu, T. Wang, Z. Zhang, T. Shen, X. Rong, B. Sheng, L. Yang, D. Li, J. Wei, S. Sheng, X. Li, Z. Chen, R. Tao, Y. Yuan, X. Yang, F. Xu, J. Zhang, K. Liu, X.-Z. Li, B. Shen, X. Wang, *Adv. Mater.* **2022**, 34, 2106814.
- [66] Q. Chen, K. Yang, M. Liang, J. Kang, X. Yi, J. Wang, J. Li, Z. Liu, *Nano Convergence* **2023**, 10, 39.
- [67] J. H. Choi, H. Y. Ahn, Y. S. Lee, K. Park, T.-H. Kim, K. S. Cho, C. W. Baik, S. I. Kim, H. Yoo, E. H. Lee, B. L. Choi, S.-D. Kim, Y.-W. Kim, M. Kim, S. Hwang, *J. Mater. Chem.* **2012**, 22, 22942.
- [68] P. An, L. Zhao, S. Zhang, L. Liu, R. Duan, X. Wei, H. Lu, J. Wang, J. Li, *Phys. Status Solidi C* **2016**, 13, 200.
- [69] M. Hiroki, H. Asahi, H. Tampo, K. Asami, S. Gonda, *J. Cryst. Growth* **2000**, 209, 387.
- [70] G. Nouet, P. Ruterana, H. Tampo, H. Asahi, *Phys. Status Solidi C* **2003**, 1, 409.
- [71] Y. Sato, A. Fujiwara, S. Ishizaki, S. Nakane, Y. Murakami, *Phys. Status Solidi A* **2017**, 14, 1600151.
- [72] S.-E. Park, D.-J. Kim, *J. Cryst. Growth* **2003**, 252, 87.
- [73] G. Nouet, P. Ruterana, H. Tampo, H. Asahi, *J. Phys.: Condens. Matter* **2002**, 14, 12697.
- [74] K. Yamada, H. Asahi, H. Tampo, Y. Imanishi, K. Ohnishi, K. Asami, *Appl. Phys. Lett.* **2001**, 78, 2849.
- [75] X.-Q. S. Ide, S.-H. C. Shimizu, S. Hara, H. Okumura, S. Sonoda, S. Shimizu, *Jpn. J. Appl. Phys.* **2000**, 39, L16.
- [76] J. Lu, D. Denninghoff, R. Yeluri, S. Lal, G. Gupta, M. Laurent, S. Keller, S. P. DenBaars, U. K. Mishra, *Appl. Phys. Lett.* **2013**, 102, 23.
- [77] A. Pandey, J. Min, M. Reddeppa, Y. Malhotra, Y. Xiao, Y. Wu, K. Sun, Z. Mi, *Nano Lett.* **2023**, 23, 1680.
- [78] A. Pandey, Y. Xiao, M. Reddeppa, Y. Malhotra, J. Liu, J. Min, Y. Wu, Z. Mi, *Appl. Phys. Lett.* **2023**, 122, 15.
- [79] J.-W. Min, H.-Y. Hwang, E.-K. Kang, K. Park, C.-H. Kim, D.-S. Lee, Y.-D. Jho, S.-Y. Bae, Y.-T. Lee, *Jpn. J. Appl. Phys.* **2016**, 55, 05FB03.
- [80] S. Hasegawa, S. Nishida, T. Yamashita, H. Asahi, *Thin Solid Films* **2005**, 487, 260.
- [81] J.-W. Min, S.-Y. Bae, W.-M. Kang, K. W. Park, E.-K. Kang, B.-J. Kim, D.-S. Lee, Y.-T. Lee, *CrystEngComm* **2015**, 17, 5849.
- [82] S.-Y. Bae, J.-W. Min, H.-Y. Hwang, K. Lekhal, H.-J. Lee, Y.-D. Jho, D.-S. Lee, Y.-T. Lee, N. Ikarashi, Y. Honda, H. Amano, *Sci. Rep.* **2017**, 7, 45345.
- [83] A. Pandey, J. Min, Y. Malhotra, M. Reddeppa, Y. Xiao, Y. Wu, Z. Mi, *Photonics Res.* **2022**, 10, 2809.
- [84] Y. Wu, X. Liu, A. Pandey, P. Zhou, W. J. Dong, P. Wang, J. Min, P. Deotare, M. Kira, E. Kioupakis, Z. Mi, *Prog. Quantum Electron.* **2022**, 85, 100401.
- [85] K. J. Lee, J.-W. Min, B. Turedi, A. Y. Alsalloum, J.-H. Min, Y. J. Kim, Y. J. Yoo, S. Oh, N. Cho, R. C. Subedi, S. Mitra, S. E. Yoon, J. H. Kim, K. Park, T.-H. Chung, S. H. Jung, J. H. Baek, Y. M. Song, I. S. Roqan, T. K. Ng, B. S. Ooi, O. M. Bakr, *ACS Energy Lett.* **2020**, 5, 3295.
- [86] J. H. Kim, N. Shepherd, M. R. Davidson, P. H. Holloway, *Appl. Phys. Lett.* **2003**, 83, 4279.
- [87] J. H. Kim, P. H. Holloway, *Appl. Phys. Lett.* **2004**, 85, 1689.
- [88] A. Prabaswara, J.-W. Min, R. C. Subedi, M. Tangi, J. A. Holguin-Lerma, C. Zhao, D. Priante, T. K. Ng, B. S. Ooi, *Nanoscale Res. Lett.* **2019**, 14, 45.
- [89] A. Prabaswara, H. Kim, J.-W. Min, R. C. Subedi, D. H. Anjum, B. Davaasuren, K. Moore, M. Conroy, S. Mitra, I. S. Roqan, T. K. Ng, H. N. Alshareef, B. S. Ooi, *ACS Nano* **2020**, 14, 2202.
- [90] K. Hantanasirisakul, M.-Q. Zhao, P. Urbankowski, J. Halim, B. Anasori, S. Kota, C. E. Ren, M. W. Barsoum, Y. Gogotsi, *Adv. Electron. Mater.* **2016**, 2, 1600050.

- [91] Z. Wang, H. Kim, H. N. Alshareef, *Adv. Mater.* **2018**, *30*, 1706656.
- [92] T. R. Kuykendall, M. V. P. Altoe, D. F. Ogletree, S. Aloni, *Nano Lett.* **2014**, *14*, 6767.
- [93] A. Prabaswara, J.-W. Min, C. Zhao, B. Janjua, D. Zhang, A. M. Albadri, A. Y. Alyamani, T. K. Ng, B. S. Ooi, *Nanoscale Res. Lett.* **2018**, *13*, 41.
- [94] K. J. Lee, Y. J. Kim, J.-H. Min, C. H. Kang, R. C. Subedi, H. Zhang, L. Al-Maghrabi, K. Park, D. Ahn, Y. Pak, T. K. Ng, Y. M. Song, B. S. Ooi, O. M. Bakr, J. Min, *Adv. Electron. Mater.* **2024**, *10*, 2400095.
- [95] J. W. Shon, J. Ohta, K. Ueno, A. Kobayashi, H. Fujioka, *Appl. Phys. Express* **2014**, *7*, 085502.
- [96] X. Xu, J. Smajic, K.-h. Li, J.-W. Min, Y. Lei, B. Davaasuren, X. He, X. Zhang, B. S. Ooi, P. M. F. J. Costa, H. N. Alshareef, *Adv. Mater.* **2022**, *34*, 2105190.
- [97] Y. Yin, B. Liu, Q. Chen, Z. Chen, F. Ren, S. Zhang, Z. Liu, R. Wang, M. Liang, J. Yan, J. Sun, X. Yi, T. Wei, J. Wang, J. Li, Z. Liu, P. Gao, Z. Liu, *Small* **2022**, *18*, 2202529.
- [98] K. Chung, S. I. Park, H. Baek, J.-S. Chung, G.-C. Yi, *NPG Asia Materials* **2012**, *4*, e24.
- [99] W.-C. Miao, F.-H. Hsiao, Y. Sheng, T.-Y. Lee, Y.-H. Hong, C.-W. Tsai, H.-L. Chen, Z. Liu, C.-L. Lin, R.-J. Chung, Z.-T. Ye, R.-H. Horng, S.-C. Chen, H.-C. Kuo, J.-H. He, *Adv. Opt. Mater.* **2024**, *12*, 2300112.
- [100] V. W. Lee, N. Twu, I. Kymissis, *Inf. Disp.* **2016**, *32*, 16.
- [101] H. Chen, G. Tan, S.-T. Wu, *Opt. Express* **2017**, *25*, 33643.
- [102] Y. Huang, G. Tan, F. Gou, M.-C. Li, S.-L. Lee, S.-T. Wu, *J. Soc. Inf. Disp.* **2019**, *27*, 387.
- [103] Y. Huang, E.-L. Hsiang, M.-Y. Deng, S.-T. Wu, *Light: Sci. Appl.* **2020**, *9*, 105.
- [104] V. Matias, C. Sheehan, J. Osinski SID Symposium Digest of Technical Papers **2024**, Vol. 55 p. 190.
- [105] A. T. Elshafey, K. M. DaVico, A. K. Rishinaramangalam, A. Rashidi, A. Aragon, D. Fezell, B. P. Gunning, C. Sheehan, V. Matias, *phys. Status Solidi A* **2020**, *217*, 1900800.
- [106] Matias, V., *In Light-Emitting Devices, Materials, And Applications XXV 2021 SPIE*, vol. 11706, p. 117060U.
- [107] Y. Liu, Z. Liu, K. M. Lau, *Optics Express* **2023**, *31*, 31300.
- [108] O. Durnan, V. Kumar, R. Alshanbari, M. Noga, I. Kymissis, *J. Soc. Inf. Disp.* **2024**, *32*, 350.
- [109] L. Qi, P. Li, X. Zhang, K. M. Wong, K. M. Lau, *Light: Sci. Appl.* **2023**, *12*, 258.
- [110] S. Barik, D. Liu, J. Brown, M. Wintrebert-Fouquet, A. J. Fernandes, P. P.-T. Chen, Q. Gao, V. Chan, I. Mann, *In Light-Emitting Devices, Materials, And Applications 2019*, SPIE, vol. 10940, pp. 181–188.
- [111] D. Liang, B. Jiang, Z. Liu, Z. Chen, Y. Gao, S. Yang, R. He, L. Wang, J. Ran, J. Wang, P. Gao, J. Li, Z. Liu, J. Sun, T. Wei, *Adv. Sci.* **2024**, *11*, 2305576.
- [112] Corning Incorporated, *EAGLE XG Slim Glass Substrates | Glass Substrate For LCD & Evolving Displays*, <https://www.corning.com/worldwide/en/products/display-glass/products/eagle-xg-slim.html> (accessed: May 2025).
- [113] A. G. Schott, *Technical Details Of AF 32@ Eco*, <https://www.schott.com/en-us/products/af-32-eco-p1000308/technical-details> (accessed: May 2025).
- [114] Abrisa Technologies, *AGC EN-A1 Alkali-Free Boro-Aluminosilicate Glass*, <https://abrisatechnologies.com/glass-materials/agc-en-a1/> (accessed: May 2025).
- [115] ASTM International, *ASTM E228-22 Standard Test Method For Linear Thermal Expansion Of Solid Materials With A Push-Rod Dilatometer*, <https://store.astm.org/e0228-22.html> (accessed: May 2025).
- [116] ASTM International, *ASTM C338-24 Standard Test Method For Softening Point Of Glass*, <https://store.astm.org/c0338-24.html> (accessed: May 2025).
- [117] ASTM International, *ASTM C225-85(2022) Standard Test Methods For Resistance Of Glass Containers To Chemical Attack*, <https://store.astm.org/c0225-85r22.html> (accessed: May 2025).
- [118] ASTM International, *ASTM C1036-25 Standard Specification For Flat Glass*, <https://store.astm.org/c1036-25.html> (accessed: May 2025).
- [119] ASTM International, *ASTM C657-24 Standard Test Method For Volume Resistivity Of Glass*, <https://store.astm.org/c0657-24.html> (accessed: May 2025).
- [120] Corning Incorporated, *Corning | Materials Science Technology And Innovation*, <https://www.corning.com/worldwide/en.html> (accessed: May 2025).
- [121] AGC Inc., *The AGC Group Creates New Value In The Fields Of Glass, Electronics, Chemicals And Ceramics*, <https://www.agc.com/en/> (accessed: May 2025).
- [122] A. G. Schott, SCHOTT | Pioneer the impossible, <https://www.schott.com/en-gb> (accessed: May 2025).
- [123] T. Li, C. Liu, Z. Zhang, B. Yu, H. Dong, W. Jia, Z. Jia, C. Yu, L. Gan, B. Xu, *AIP Advances* **2018**, *8*, 4.
- [124] J. Yu, Z. Hao, J. Wang, J. Deng, W. Yu, L. Wang, Y. Luo, Y. Han, C. Sun, B. Xiong, H. Li, *J. Alloys Compd.* **2019**, *783*, 633.
- [125] D. P. Borisenko, A. S. Gusev, N. I. Kargin, P. L. Dobrokhoto, A. A. Timofeev, V. A. Labunov, N. G. Kovalchuk, M. M. Mikhaliik, I. V. Komissarov, *Jpn. J. Appl. Phys.* **2019**, *58*, SC, SC1046.
- [126] Q. Chen, K. Yang, B. Shi, X. Yi, J. Wang, J. Li, Z. Liu, *Adv. Mater.* **2023**, *35*, 2211075.



Jungwook Min is an assistant professor in the Department of Optical Engineering at Kumoh National Institute of Technology (KIT), Republic of Korea. He received his Ph.D. in Physics and Photon Science from the Gwangju Institute of Science and Technology (GIST). His research focuses on the epitaxial growth of III-nitrides and oxide semiconductors, their heterogeneous integration via thin-film exfoliation, and hetero-interface engineering. He specializes in material characterization and the development of photonic and electronic devices based on wide-bandgap semiconductors.



Kwangwook Park is an associate professor in the Division of Advanced Materials Engineering at Jeonbuk National University (JBNU), Republic of Korea. He received his Ph.D. in Information and Communications (now Electrical Engineering and Computer Science) from Gwangju Institute of Science and Technology (GIST) and was a postdoctoral researcher in the Materials Physics Group at the National Renewable Energy Laboratory (NREL), USA. His research focuses on the characterization and molecular beam epitaxy growth of III-P/As, II-Se/Te, and III-N compound semiconductors, as well as sputter deposition of II-IV-N₂ semiconductors for optoelectronic applications.